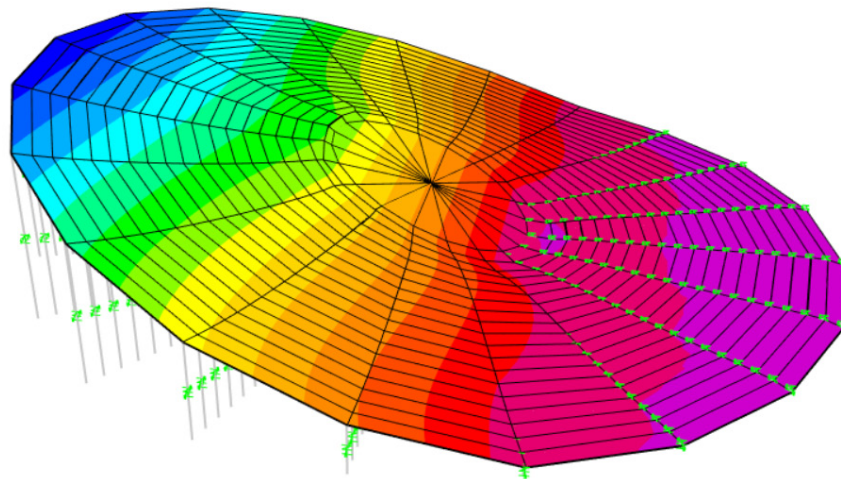




LUND
UNIVERSITY



PARAMETRIC DESIGN OF WIND TURBINE FOUNDATIONS

Enhancing Efficiency Through Automated Modeling

EMIL HOLST SNECKENBORG

Structural
Mechanics

Master's Dissertation

DEPARTMENT OF CONSTRUCTION SCIENCES
DIVISION OF STRUCTURAL MECHANICS

ISRN LUTVDG/TVSM--24/5276--SE (1-85) | ISSN 0281-6679

MASTER'S DISSERTATION

PARAMETRIC DESIGN OF WIND TURBINE FOUNDATIONS

Enhancing Efficiency Through Automated Modeling

EMIL HOLST SNECKENBORG

Supervisors: Professor **KENT PERSSON**, Division of Structural Mechanics, LTH
and **BABAK NAVID**, MSc, AFRY.

Assistant Supervisor: **LINUS ANDERSSON**, Postgraduate Student, Division of Structural Mechanics, LTH.

Examiner: **SUSANNE HEYDEN**, Associate Professor, Division of Structural Mechanics, LTH.

Copyright © 2024 Division of Structural Mechanics,
Faculty of Engineering LTH, Lund University, Sweden.

Printed by V-husets tryckeri LTH, Lund, Sweden, August 2024 (PI).

For information, address:

Division of Structural Mechanics,
Faculty of Engineering LTH, Lund University, Box 118, SE-221 00 Lund, Sweden.

Homepage: www.byggmek.lth.se

Abstract

The escalating concerns surrounding climate change have intensified the focus on the renewable energy market, with initiatives aimed at energy security, CO₂ emissions reduction, and sustainability. Wind turbines, considered a key component of renewable energy solutions, have seen significant investment growth globally. However, challenges persist, including the environmental impact of construction and economic factors affecting profitability. This thesis aims to address these challenges by developing an automated script for wind turbine foundation design, contributing to streamlining processes in the renewable energy sector.

In the development of the script the API documentation for SAP2000 has been utilized to automate the modeling of the foundation. The foundation is modeled with thick area elements to replicate the sloped geometry and properties of the foundation. FEM-analysis for different load cases was performed on the model in order to output sectional moments, normal and shear forces. The forces were used in order to design required reinforcement in the radial and tangential direction at the top and bottom edges of the foundation. This was performed with the sandwich model. Further, design of required shear reinforcement was incorporated into the script. As a result, the script outputs required reinforcement in tangential, radial and shear direction to guarantee structural integrity. Fatigue assessment was carried out using Markov matrices to verify that the cumulative damage of is below the value of 1.

The foundation design has not examined the impact of the anchor cage. Only simplifications of constraining it as a rigid body has been carried out. This implies that a more thorough analysis of the anchor cage's impact on the foundation is necessary before relying fully on the script's results.

Simpler calculations for the bearing and sliding capacity, along with overturning risk, were conducted based on established guidelines. Consequently, the modeling primarily emphasizes the behavior of the foundation rather than the soil itself.

Sammanfattning

Oro kring klimatförändringar har ökat fokus på den förnybara energimarknaden, med initiativ som syftar till energisäkerhet, minskning av CO₂-utsläpp och hållbarhet. Vindkraftverk anses vara en nyckelkomponent i förnybara energilösningar, har sett betydande investeringstillväxt globalt. Utmaningar kvarstår dock, såsom miljöpåverkan från konstruktion och ekonomiska faktorer som påverkar lönsamheten. Denna Masteruppsats syftar till att adressera dessa utmaningar genom att utveckla ett automatiserat skript för dimensionering av vindkraftverksfundament, vilket kan bidra till att effektivisera processer inom den förnybara energisektorn.

I utvecklingen av skriptet har API-dokumentationen för SAP2000 använts för att automatisera modelleringen av fundamentet. Fundamentet modellerades med tjocka skal-element för att efterlikna den lutande geometrin och egenskaperna hos fundamentet. FEM-analys för olika lastfall utfördes på modellen för att generera snittmoment och -krafter. Dessa krafter användes för att dimensionera nödvändig armering i radiell- och tangentiell riktning för fundamentets sektioner. Detta utfördes med den så kallade Sandwich-modellen. Vidare integrerades dimensionering av nödvändig tvärkraftsarmering i skriptet. Som ett resultat genererar skriptet rekommenderad minimal armeringsarea för sektioner av fundamentet i alla riktningar, för att garantera tillräcklig bärförmåga. Utmattningsbedömning utfördes med hjälp av Markov-matriser för att verifiera att den ackumulerade skadan på den mest utsatta armeringen understiger värdet 1.

Inverkan av bultkorgen för fundamentet har inte undersökts i detalj, med undantag för förenklingen där den behandlats som en stel kropp. Således bör en mer grundlig analys av bultkorgens inverkan på fundamentet göras innan skriptets resultat används.

Enklare beräkningar grundens bärförmåga och risk för glidning, och risk för vältnings, genomfördes enligt etablerade riktlinjer från DNV-RISØ. Modelleringen fokuserar således främst på beteendet hos fundamentet snarare än marken.

Acknowledgements

I would like to express my deepest appreciation to Babak Navid for continuously taking the time to answer my questions. In addition, I would like to show my gratitude to my supervisor, Kent Persson, who seems to trust me enough to get this thesis done in time for my graduation.

Many thanks to AFRY, Daniel Lundström, who provided the opportunity to increase my knowledge in scripting, structural design, and also providing me with equipment to do my work. I am also thankful for Farshid Zamiri.

Thanks should also go to Linus Andersson which always have been helpful during my masters at Lunds Tekniska Högskola.

Lastly, I would like to acknowledge Department of Structural Mechanics for their unwavering support throughout the Master's program. Their willingness to respond to any inquiries regarding structural design has always been warmly received.

Notations and Symbols

Latin letters

A_{eff} - Effective area
 A_{sw} - Cross-sectional area of the shear reinforcement
 $A_{x,top}$ - Reinforcement in radial direction to the top edge
 $A_{x,bot}$ - Reinforcement in radial direction to the bottom edge
 $A_{y,top}$ - Reinforcement in tangential direction the top edge
 $A_{y,bot}$ - Reinforcement in radial direction to the bottom edge
 D - Depth of burial or cumulative damage
 G_1 - Shear modulus for first soil layer
 G_2 - Shear modulus for second soil layer
 H - Height of the foundation
 H_{Ed} - Horizontal design load
 H'_{Ed} - Equivalent horizontal force
 H_{soil} - Height of the soil to second layer
 K_V - Vertical spring stiffness
 K_H - Horizontal spring stiffness
 M_{stb} -Stabilizing moment
 M_{Ed} - Design bending moment
 $N_{f,i}$ - Cycles to failure
 R - Radius of the foundation
 R_{Rd} - Total bearing resistance
 R_k - Sliding capacity
 V_{Ed} - Shear design load
 V_{Rd} - Shear resistance

b_e - Effective width
 c - Characteristic cohesion
 e_d - Eccentricity
 f_{yd} - Design yield stress of reinforcement
 f_{ywd} - Design yield strength of the shear reinforcement
 h_{comp} - Height of compressed segment
 l_e - Effective length
 n_i - Measured cycles
 q_{ult} - Ultimate bearing capacity
 $T_{Areaelement}$ - Thickness of area element.
 d_{conc} - Concrete cover
 d_{top} - Reinforcement diameter top
 d_{bottom} -Reinforcement diameter bottom
 z - Distance between reinforcements

Greek letters

α - The angle of the base of the foundation to horizontal

α_{comp} - Width of the compressed area

θ_{comp} - Angle of compressed segment

ν_1 - Poisson's ratio

μ - Friction angle

σ_{allow} - Design load bearing capacity

σ_s - Maximum stress

$\Delta\sigma_R$ - Stress Range

ϕ_k - Characteristic friction angle

$\gamma_{surcharge}$ - Soil unit weight

γ_G - Partial safety factor

Contents

Abstract	I
Sammanfattning	III
Acknowledgements	V
Notations and Symbols	VII
Table of Contents	X
1 Introduction	1
1.1 Background	1
1.2 Goal and Objectives	2
1.2.1 Project Goal	3
1.2.2 Limitations	4
2 Theory	7
2.1 Wind loads	7
2.2 Standards and Design codes	9
2.2.1 Turbine classes	10
2.2.2 Design loads	10
2.3 Foundations	11
2.4 Wind Turbine Stability	12
2.4.1 Foundation design considerations	13
2.4.2 Bearing capacity	13
2.4.3 Sliding	15
2.4.4 Subgrade modulus	15
2.4.5 Stiffness	16
2.5 Structural foundation design	18
2.5.1 Concrete	18
2.5.2 Reinforcement	18
2.5.3 Shear reinforcement	22
2.5.4 Fatigue	24
2.5.5 Fatigue Estimation methods	25
2.5.6 Crack width	30
2.6 Modeling foundations	30
2.6.1 Finite element method	30
3 Methods used in the scripting	33
3.1 FE-Modelling	33

3.2	Verifications and model estimates	36
3.2.1	Soil bearing capacity in drained conditions	37
3.2.2	Sliding capacity	38
3.2.3	Overturning Control	38
3.3	Reinforcement Design	40
3.3.1	Combined in plane and flexural bending reinforcement	40
3.3.2	Shear Reinforcement	41
3.3.3	Punching	43
3.4	Fatigue	44
4	Results	47
4.1	Definitions	47
4.2	Spring stiffness	49
4.3	Bearing capacity	49
4.4	Sliding capacity	51
4.5	Overturning capacity	51
4.6	Convergence study	52
4.7	Moments and Normal forces	53
4.8	Tangential and radial reinforcement	56
4.8.1	Shear Reinforcement	57
4.8.2	Punching	58
4.9	Fatigue	59
5	Discussion	63
5.1	Background	63
5.1.1	Bearing capacity and rotation	63
5.1.2	Convergence study	63
5.1.3	Modelling	63
5.1.4	Loads	64
5.1.5	Springs	65
5.1.6	Reinforcement	65
5.2	Fatigue	67
5.3	Final words	68
	Bibliography	69
	A IEC Design load cases	71
	B Bearing capacity	73
	C Shear reinforcement	75
	D Reinforcement example for sandwich model	77
	E Load case results	79

1 Introduction

1.1 Background

The escalating concerns surrounding the climate change have exerted significant pressure on the renewable energy market. Issues regarding energy securities, CO₂ emission reduction, sustainability, and global warming are recurrent topics of discussion in today's society. In developed countries, there are incentives to adopt sustainable practices, ranging from ESG investment funds, recyclable building materials, to transportation, energy-efficient lighting, and renewable energy in the form of solar power plants and wind turbines. The common objective shared among these initiatives is to minimize environmental impact and foster sustainable living for future generations to come and simultaneously capitalize on the market trend.

The view that wind turbines can accommodate one of the future renewable energy sources is strongly supported by the amounts of investments made in recent years. According to Wood Mackenzie et al. [1] the first half of 2023 has had an increase in orders of 12% to that of the previous years and the growth of wind turbine investment has been increasing since 2011, with a slight decrease in 2018 [2]. Although statistics are adjusted to fit forecast to please the readers and investors, there is no denial in that wind turbine is a topic that has mobilized a community to change the way of thinking. Specially when referring to sustainable solutions for the renewable energy market.

Wind turbines represents one of the most significant innovations in renewable energy today. However, despite their promise, the construction contribute to CO₂ emissions. The substantial amounts of concrete required for stabilizing the wind turbine, coupled with heavy reinforcement necessary to prevent cracking and fatigue load leaves a significant footprint. Nevertheless, wind energy production presents a comparatively lower environmental impact than many other energy productions methods and is probably here to stay.

Recent advances in the field of structural engineering, aerodynamics and meteorology have propelled the wind turbine industry to reach new impressive levels on efficiency, size an reliability. These technological breakthroughs, coupled with favorable economic conditions and supportive policy environments, have ignited investments for several years and the optimism remains. China, a global leader of wind turbines has developed remarkable off shore wind turbines with a reach of rotor-blades measuring +250 meters and generating between 6-10 megawatts of power. Additionally, China's leadership in the renewable energy sector is set to make a significant impact globally. Projections indicate that by 2028, China will be responsible for 60% of the world's operational renewable energy capacity, including solar power [3].

For the first time in history, 2023, the wind industry passed 1 TW (TerraWatt) of

installed wind capacity and the ambition to install another TW within this decade is according to the Global Wind Council et al. [4] on the right way. However, challenges in the wind power industry have become more relevant than ever. Turbine manufacturers in Europe and North America have faced negative net margins for seven consecutive quarters due to factors such as increased interest rates, limited raw materials, supply chain disruptions, and extended permitting timelines. The costs have reportedly surged by 20 % compared to previous year, leading to cancellation or postponement of projects in the United Kingdom and United States due to lack of justification of the expenditure [3].

Although there are increases in project cancellation and postponement, it is my belief that the demand and willingness to produce wind turbines remains as soon as a more attractive economy is present, referring to the decrease in interest rates. Assuming that the increased demand in wind turbines continues it's logical for construction companies and designers to lower costs to reach profitability. Furthermore, high demands put pressure on faster design while still continuously guaranteeing reliability and optimized solutions. The conservative construction industry still fails to provide automated solutions and digitalize the industry. One reason for this could be that projects in the sector of infrastructure is often times different from one another. However, wind turbines are slightly similar, therefore automated modeling can greatly increase efficiency for employees and companies. In this matter we can keep up with the high paced market and thus reach EU's climate goals and simultaneously reach profitability. Naturally, there are several other factors that influence the installation of wind turbines. Automated design is only a small part of a complex chain link and there are several other processes that needs to be further streamlined to achieve efficient development of wind-turbines.

This thesis will concentrate on analyzing and examining the design aspects of wind turbine foundations. No investigations or evaluations will be undertaken regarding rotor blades, tower structures, or mechanical components. The foundation plays a critical role in ensuring the wind turbine's stability and transferring cyclic loads from the wind through the tower into the ground. The type of foundation employed determines how the load is distributed to the ground. Consequently, this thesis will solely focus on gravitational foundations. The study will encompass various aspects such as geometric considerations, fatigue analysis in reinforcement, design of reinforcement, and assessment of soil bearing capacity.

1.2 Goal and Objectives

Despite advancements being made in the construction industry it still lacks automation. Automating the design process can significantly enhance efficiency, especially for repetitive tasks like those involved in wind turbine foundation modelling. Given the repetitive nature of wind turbine foundations, companies can capitalize by developing and implementing automated scripting. Such automation can save considerable amount of time by managing parameters such as material properties, geometry, and load conditions. Further, optimization algorithms can be employed to not only enhance cost-effectiveness, but also minimize environmental impact, particularly in

terms of reducing CO_2 emissions.

1.2.1 Project Goal

This thesis is meant to formulate an understanding on how foundation design of wind turbines can be automatically modeled. It will feature key aspects of modelling, critical means and importance of foundation design for wind turbines. The modeling will be issued with the help of the Finite Element software SAP2000 to receive data of section forces of the foundation. Reinforcement design will further be carried out from data output according EN 1992-1-1:2005, among other literature.

To approach this task an automated Python script to model the foundation in SAP2000 will be written to extend the possibility to accommodate different configurations of parameters, hence accomplishing a broader use of this thesis. In addition, the thesis aims to ignite future automation processes and Python scripting in the field of structural engineering.

Objective

In order to achieve this goal, a clear objective has been established:

- Develop a script in Python to automate the modeling in Finite Element Software SAP2000 that enables trials of varied configurations.
- Design reinforcement and concrete from software results.
- Verify Fatigue from Markov Matrices, using rain-flow counting analysis and Palmgren-Miners Rule
- Develop an automated script to draw a parametric model in Tekla structures based on the results from the main script.

Scope

The scope of this investigation is a parametric study of gravitational foundations for wind turbines. It will focus on the development of an automated script programmed to generate inputs necessary for Finite Element software to run simulations. This script will incorporate parameters such as turbine specifications, environmental conditions, and soil properties to ensure accurate modeling. Using industry-standard FEM software, simulations will be performed to analyze the structural behavior of the wind turbine foundation under various loading conditions, including static and dynamic loads. This will assess the stress distribution, deformations, and fatigue life to optimize the design. Based on the results obtained from the simulations, the thesis will investigate the reinforcement needed for the foundation to withstand the applied loads

and ensure long-term structural stability. This will involve a detailed analysis of sectional forces and fatigue verification. Life predictions will be made to assess structural integrity, taking into account the effects of cyclic loading.

1.2.2 Limitations

The primary focus of this thesis has been on the development of a script aimed at automating the process of modeling and designing a wind turbine foundation. Although certain aspects of the thesis delve into the theoretical framework surrounding the design of the foundation and the associated assumptions, the main emphasis has been on the development and implementation of the script itself.

The modeling of the foundation has encountered several limitations, primarily concerning the representation of the anchor cage. In the model, the anchor cage has been treated as having the same material properties as the surrounding concrete, thus disregarding its steel-heavy properties. Despite this simplification, it has been constrained to act as a rigid body, providing results that are motivated to align with a more detailed model. Additionally, the anchoring between the anchor cage and the foundation has been completely neglected in the current implementation of the script, hence results close to anchor cage, referred to as the *PedestalGroup* should be treated with caution. This presents an area for future improvement and refinement in subsequent versions of the script.

The reinforcement design is not fully detailed, referring to specific anchoring lengths and arrangement. Instead, the script outputs a recommendation of required reinforcement per meter at the top and bottom for every group. It is therefore left to the final designer to determine how this requirement will be fulfilled. Given this, an external script could be developed to handle arrangement and drawings for optimization purposes.

Results of modeling with shell elements instead of solids has not been compared, which would strengthen the result of this thesis substantially. With this being said, correctness of modeling with thick area elements has solely been established on supervisors recommendation. Comparing the results to a solid model would yield significant insights, not only for this thesis but also for modeling in general, a topic that could warrant its own thesis

Fatigue assessment for the reinforcement has been confirmed using the Palmgren-Miners Rule. The Wöhler curve employed for this method corresponds to detail category 160, a simplification of the actual Wöhler curve for reinforced concrete. No investigation into concrete degradation over time has been conducted. The fatigue assessment was carried out using rainflow counting methods, but without the associated mean stress range to each stress range. This limitation impacts the accuracy of the fatigue assessment.

In this study, it was initially intended to apply the dead load separately before gradually increasing the applied load for the analysis of structures under nonlinear loading conditions. However, due to practical constraints and time limitations, this approach

was not implemented in the current thesis.

2 Theory

At first glance, wind turbines are defined as a simple structure. With components such as a tower, foundation, rotor blades, and mechanical head, they indeed represent fairly straightforward structures to analyze. Wind speed is converted to energy and the wind loads are transferred through the tower into the foundation, where the distributions of loads are borne by the soil. However, due to the harsh conditions subjected to the turbines engineers can't tread lightly in this field. Hurricanes, heavy storms, earthquakes and swell are the first thought of concerns. Yet, even the normal day-to-day condition pose problems. The alternating loads produced by the wind combined with a rotor of blades are concerns for material fatigue, a term used to describe exhausting material.

The large size of a wind turbine has its reasons, which becomes apparent when addressing low density air. As the wind makes contact with the rotor-blades in high speeds the air density lowers. As the air becomes less dense the amount of energy to be harnessed from the wind is reduced. To achieve higher output of energy a larger covering area is therefore required, hence making the rotor-blades longer. Naturally, components that support the rotation of the blades need to increase too. The large structures are defined as elastic which can create complex behaviours for vibrating scenarios. Although elastic behaviour ensures successful fatigue life it can lead to resonances and high dynamic load components [5].

The components must not only withstand cyclic loading but also endure extremely high loads. These loads may occur intermittently throughout the wind turbine's lifetime, sometimes even simultaneously with external forces. To gain a comprehensive understanding of wind turbine functionality, it is essential to investigate critical aspects of loading scenarios to prevent malfunction. The presence of various external loads, occurring with different amplitudes and configurations, complicates the design process and stability assurance. Structural engineers employ a tool known as *load cases* that handles configurations of worst-case scenarios and incorporating safety factors.

2.1 Wind loads

One of the most crucial aspects of a wind turbine is the wind load. The loads can be categorized into steady loads and cyclical loads. Steady loads refer to the mean wind speed that the wind turbine is subjected to. The unsteady loads can further be divided into subcategories, cyclic loads and non-cyclic. The cyclic loads originate from phenomena such as cross winds, vertical wind shear, tower draft and tower shadow. The non-cyclic loads refer to turbulence and is harder to recognize [5].

Wind shear: The wind shear phenomenon is a widely used phenomenon not only in wind turbine design, but also for buildings of several storeys. It refers to that

load amplitudes increases with the height of the structure. This phenomenon has been determined to be dependent on earth's surface roughness. The Hellman power equation 2.1 describes the wind speed change with height.

$$u(z) = u(z_0) \left(\frac{z}{z_0} \right)^a \quad (2.1)$$

Using the wind shear phenomenon suggest the reason to why wind turbine towers are made as tall as feasible. In this way one can lower the cost per unit power. Naturally, exceeding heights is costly hence there is an optimal level for cost efficiency.

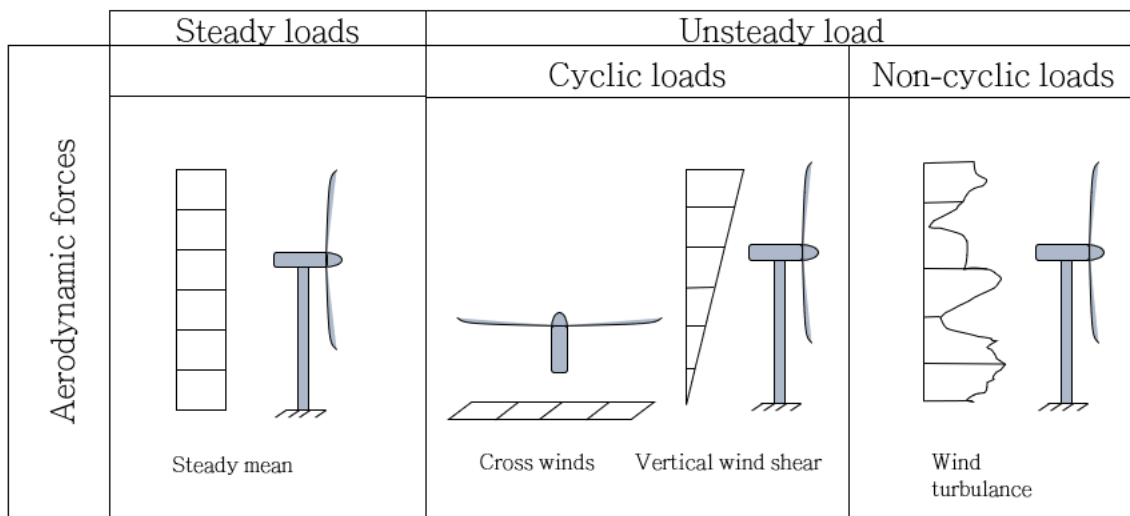


Figure 2.1: Illustration of the categorized loads for a wind turbine.

Cross winds is a similar cyclic load to that of the wind shear phenomena. The asymmetrical wind speed crossing the wind turbines rotor-blades is highly complex. The crossing wind affects the rotor-blades yaw moment depending on the angle of attack of the wind, changing the wind direction rapidly [5]. This is more of a concern regarding rotor-blades than tower.

Tower Interference implies imposition of additional loads on turbine components. When the wake of one turbine interacts with downstream turbines, it creates turbulent airflow patterns that subject these turbines to fluctuating wind conditions. These fluctuations can result in dynamic loading on the turbine tower, blades, and other structural elements, increasing the stress experienced by these components.

The wind **turbulence** and gusts are short term fluctuations of the wind speed. These are the non-cyclic loads that increase the amplitude of wind load for a brief moment and is critical when evaluating extreme load cases. Wind load fluctuations are particularly significant in the context of fatigue strength design. Addressing these fluctuations is crucial to ensure that wind turbine structures can withstand the repetitive stress of varying wind conditions over time. To accurately assess these fluctuations, engineers commonly employ stochastic models, see 2.5.5.

2.2 Standards and Design codes

The design of wind turbines has reached a international standard with certain national specifications. During the early beginnings of the eighties initial development of standardization for wind turbine design was being implemented. This was later undertaken by the International Electrotechnical commission (IEC) in 1988, including national standards from Sweden, Denmark and the US [5].

Among the design codes utilized are the national annex Swedish Standards Institutes (SIS) and Eurocode (EN). Eurocode, a comprehensive set of European standards for structural design, ensures safety, durability, and performance consistency across European Union member states, similar to the International Electrotechnical Commission (IEC). Further the EN is also used for the geotechnical design.

Alongside Eurocode (EN), the International Electrotechnical Commission (IEC) plays a crucial role in the design and understanding of wind turbine materials. The IEC, developed by global experts and approved for global publication, serves as a comprehensive guide for users to ensure reliable design standards.

The IEC establishes regulations covering safety requirements, design specifications, and measurement techniques, among other aspects. These regulations are essential considerations during the planning, construction, and maintenance of wind turbines according to IEC standards.

Today, many manufacturers provide the design loads for their products to clients. The design loads follow the IEC 61400 standards and include dynamic behaviour of the structure while also accounting for most unfavourable cases.

Table 2.1: IEC regulations.

Standard	Description
IEC 61400-1:2005	Design requirements
IEC 61400-2:2013	Small wind turbines
IEC 61400-3:2009	Design requirements for offshore wind turbines
IEC 61400-4:2012	Design requirements for wind turbine gearboxes
IEC 61400-6:2020	Tower and foundation design requirements
IEC 61400-11:2012	Acoustic noise measurement techniques
IEC 61400-12-1:2005	Power performance measurements
IEC 61400-13:2015	Measurement of mechanical loads
IEC TS 61400-14:2005	Declaration of apparent sound power level and tonality
.	.
.	.
.	.

2.2.1 Turbine classes

Depending on the intended site placement or the type of installation, different classes are determined by IEC 61400-1-6. The classes are intended to cover a broad spectrum of applications, hence values of wind speed and fluctuations are not site specific. Instead, class type S is used where the designer or customer defines the conditions of the wind turbine.

Table 2.2: Parameters for wind turbine classes.

Wind turbine classes		I	II	III	S
v_{ref}	(m/s)	50	42.5	37.5	Values specified by designer
A	$I_{\text{ref}}(-)$		0.16		
B	$I_{\text{ref}}(-)$		0.14		
C	$I_{\text{ref}}(-)$		0.12		

v_{ref} reference wind speed average of 10 min,
 I_{ref} expected value of the turbulence intensity at 15 m/s.

The IEC 61400-1-6 provide two different types of wind conditions, normal wind conditions and extreme wind conditions. The normal wind condition refers to frequent occurring events during normal operations of the wind turbine. The extreme wind conditions refers to extreme wind recurrence period of 1-50 years.

- **Normal wind conditions**

- The normal wind profile model (NWP)
- Normal turbulence model (NTM)

- **Extreme wind conditions**

- Extreme wind speed model (EWM)
- Extreme operating gust (EOG)
- Extreme turbulence model (ETM)
- Extreme direction change (EDC)
- Extreme coherent gust with direction change (ECD)
- Extreme wind shear (EWS)

2.2.2 Design loads

The IEC-61400 provides safety factors, γ_f , for load cases to ensure structural integrity, Table 2.3. Annex A displays the cases gathered from IEC 61400-1. Explanations for the design situation, most left column in 3.4 however, is not further motivated.

Table 2.3: Safety factors γ_f provided by the IEC-61400-1.

Unfavourable loads			Favourable loads
Type of design situation			All design situations
Normal (N)	Abnormal (A)	Transport and erection (T)	
1.35	1.1	1.5	0.9

The letters explain the variation of load cases. Notation of (U) and (F) in Table A refers to analysis in the ultimate limit state and fatigue load case respectively. (U) is further classified into three subcategories, normal (N), abnormal (A) or transport and erection (T), 2.3.

- Normal (N), design load case refers to occurrence on a frequent basis within the lifetime of the turbine.
- Abnormal (A), design load case refers to a design situations where severe fault might happen. These are less likely to occur, hence a lower safety factor
- Transport and erection (T), design load case factor in the transport, assembly, maintenance and repair.

2.3 Foundations

The foundation comprises three primary components: the concrete shaped cone, reinforcement, and the steel cage to which the tower is bolted. The steel cage plays a critical role in distributing external loads from the tower and transferring them to the concrete. This prevents excessive cracking in the concrete. Reinforcement, both vertical and horizontal, is strategically integrated to compensate for concrete's poor tension properties. This comprehensive approach ensures the foundation's robustness and is essential for supporting the tower's stability and structural integrity over time.

The foundation of the wind turbine is determined from the size of the turbine tower, nacelle, rotor, and soil conditions. Depending on these factors, the load cases that involve the highest load during operation and wind speed should be considered. Depending on wind, deadweight and thrust, different configurations of the load cases needs to be established. The tilting moment is the first thing that needs to be checked [5]. It's determined from load cases according the IEC and account for the steady and unsteady loads. The task of the foundation is to prevent the overturning moment caused by the external loads from exceeding the foundation weight.

Gravitational foundations foundations or more known as gravity-based foundations are the "simplest" form of foundations. By utilizing a circular concrete slab one uses the concrete's heavy weight to prevent the wind turbine from falling. By distributing the load on a large area of the soil one can prevent settlements in soil, given that the soil has enough bearing capacity. Depending on soil conditions, it may be feasible to further lower the concrete slab by excavating and back filling the soil. By excavating and replacing the unsuitable soil with better-quality material, the foundation's stability and load-bearing capacity can be enhanced. This approach ensures that the foundation rests on a solid substrate, minimizing the risk of settlement or structural issues over time.

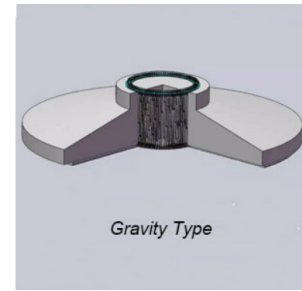


Figure 2.2: Gravity foundation.

Gravitational foundations are more cost efficient, due to eliminating the need for extensive geotechnical, study, investigations and piling. The thesis will exclusively prioritize studies on these foundation types.

Piled foundations serve as a crucial solution in cases where the soil lacks adequate bearing capacity to support the weight of wind turbines. This type of foundation involves driving piles deep into the ground, reaching down to the bedrock or relying on frictional forces between the piles and the soil for support. While piled foundations offer robust structural support, they also impose greater demands on the connections between the anchors and the concrete slab. Despite these challenges, they provide a viable solution for wind farms located in areas with insufficient soil bearing capacity. In the case of rock foundations, the anchor cage is reinforced into the rock using anchor rods, leveraging the inherent bearing capacity of the rocky terrain to anchor the foundation securely. This approach reduces the need for extensive concrete and steel reinforcement work, thereby lowering the construction costs of piled foundation wind farms [6].

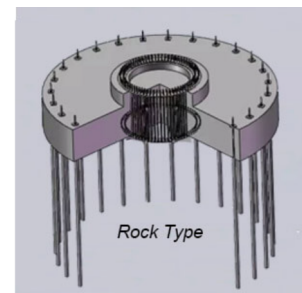


Figure 2.3: Piled foundation

Piled foundations has a greater cost due to the extensive work of doing Geotechnical reports on the ground before even continuing. Further the piling itself is work heavy, hence increasing the cost greatly with the amount of piles needed. Higher demands on connection between anchors and concrete slab but lower bearing capacity of the soil is a fact.

2.4 Wind Turbine Stability

Foundations form the bedrock of wind turbine structures, providing essential support and stability to ensure their safe and effective operation. This sub chapter explores the fundamental principles and methodologies guiding the design of these critical components.

Throughout this chapter, key factors influencing foundation design for wind turbines will be examined. From analyzing the forces exerted on the foundation to assessing soil conditions and determining bearing capacity. Each aspect plays a crucial role in ensuring the structural integrity and longevity of wind turbine installations.

By understanding the principles outlined in this chapter, engineers and stakeholders can make informed decisions when selecting foundation types, optimizing designs, and mitigating risks associated with various environmental and operational challenges.

2.4.1 Foundation design considerations

According to DNV-RISØ [7], wind turbine foundations are considered small, hence load bearing capacity formulas for idealised conditions are normally sufficient.

The forces transferred to the foundation boundary on the soil result in a vertical force V and a horizontal directed force on the foundation soil boundary H . These forces will work as design forces and their intersection with each other is defined as the load center LC, see Fig 2.4. This is necessary to describe the eccentricity of the vertical force acting relative to the center line. The eccentricity can be calculated by dividing the overturning moment M_d , produced from the wind load, by the vertical design load V_d , Eq 2.2.

$$e = \frac{M_d}{V_d} \tag{2.2}$$

When designing bearing capacity, the term effective foundation area, denoted by A_{eff} , is used. This term ensures that the geometrical center aligns with the load center, accurately representing the effective area of the foundation. Two different approaches are employed depending on whether the foundation is circular or quadratic. In Table 2.4 the two different scenarios are presented.

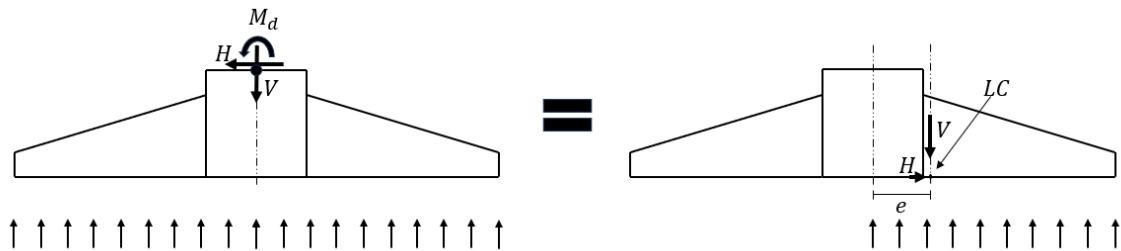


Figure 2.4: Illustration of the load center and its eccentricity.

2.4.2 Bearing capacity

Investigating the soil is necessary to provide data for specific foundation structures. The geotechnical work is divided into three parts. Geological studies, surveys, and investigations. The Geological study refers to gathering information about the soil history and its goal is to establish a basis for further detailed site investigations. [8]

Table 2.4: Effective area foundation for quadratic and circular foundations.

Scenario	Description	Major Axes
Scenario 1	Load eccentricity to one symmetry axis of the foundation. For quadratic foundations, the effective area is calculated as: $A_{eff} = b_{eff} \cdot l_{eff} \quad (2.3)$	$b_{eff} = b - 2 \cdot e$ $l_{eff} = b$
Scenario 2	Load eccentricity with respect to both symmetry axes of the foundation. For circular foundations, the effective area is determined by: $A_{eff} = 2 \left[R^2 - \arccos \left(\frac{e}{R} \right) - e \sqrt{R^2 - e^2} \right] \quad (2.4)$	$b_{eff} = l_{eff} = b - e\sqrt{2}$

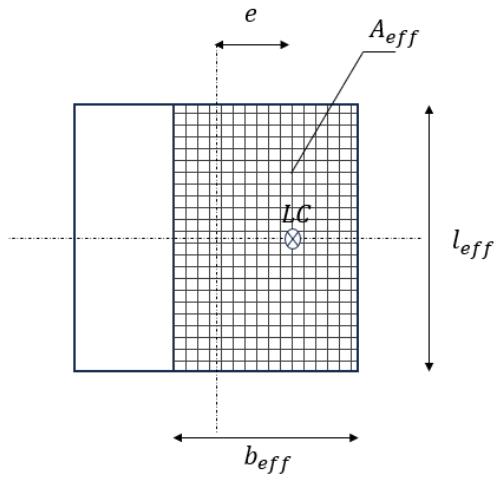


Figure 2.5: Scenario 1.

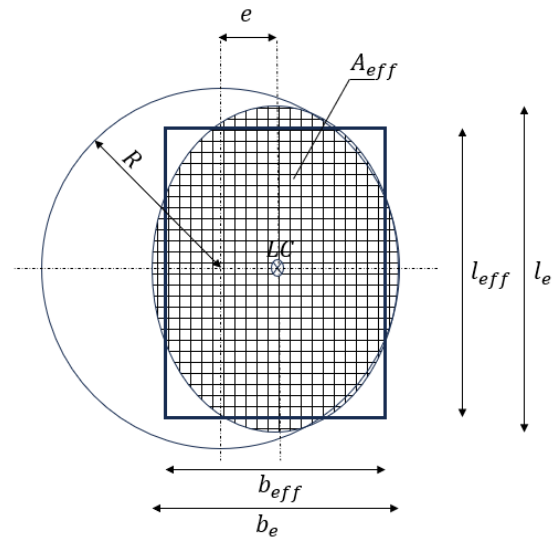


Figure 2.6: Scenario 2.

The bearing capacity of the soil is a crucial consideration in foundation design. Depending on local soil conditions, risk assessments of settlements are considered. The dimensions of the foundation can significantly be influenced by the soil condition. By increasing the surface area for load distribution, the pressure exerted on the soil decreases. Another aspect of foundation design is groundwater. Groundwater poses another challenge, potentially increasing the stresses on the foundation due to the hydrostatic pressure. The hydrostatic pressure from the groundwater emits a force

underneath the foundation pushing it upwards, complicating the foundation stability. Further, water can saturate the material, which accelerates the deterioration processes [8].

The bearing capacity under fully drained conditions can be determined by the following general formula, as expressed in Eq. 2.5:

$$q_d = \frac{1}{2} \gamma' b_{eff} N_{\gamma} s_{\gamma} i_{\gamma} + p_0 N_q s_q i_q + c_d N_c s_c i_c \quad (2.5)$$

In cases where extreme eccentricity is present, another consideration is taken into account. This involves the failure mode of the soil beneath the unloaded part of the foundation area. Equation 2.6 can be utilized for this scenario:

$$q_d = \gamma' b_{eff} N_{\gamma} s_{\gamma} i_{\gamma} + c_d N_c s_c i_c (1.05 + \tan^3 \phi) \quad (2.6)$$

The detailed explanation of the parameters are referenced in annex B.

2.4.3 Sliding

Due to the horizontal loading, investigation towards sufficient sliding resistance is necessary. Criteria according to DNV-RIS for drained, Eq.2.7 and undrained, Eq. 2.8 conditions in clay are.[7]

1. Drained Condition:

$$H < A_{eff} \cdot c + V \cdot \tan \phi \quad (2.7)$$

where H is the horizontal loading, A_{eff} is the effective area of the foundation base, c is the soil cohesion, V is the vertical load, and ϕ is the soil friction angle.

2. Undrained Condition:

$$H < A_{eff} \cdot c_{ud} \quad (2.8)$$

where c_{ud} is the design undrained shear strength, assessed based on the actual shear strength profile, load configuration, and estimated depth of potential failure surface.

Additionally, the ratio $\frac{H}{V} < 0.4$ must be verified.

2.4.4 Subgrade modulus

The rotation of a foundation due to wind loads, denoted as ϕ , is regarded as an imperfection. Although the deformation behavior in cohesive soils are typically analyzed by soil mechanics specialists, considerations of overturning effects from the tower are relevant. These considerations involve calculating both the dynamic modulus of elasticity and the static modulus for elasticity, as expressed in Equations 2.9 and 2.10.

$$c_{s,dyn} = \frac{E_{s,dyn}}{f' \cdot \sqrt{A_{foundation}}} \quad (2.9)$$

where:

Another critical consideration in deformation calculations based on second-order theory is the non-elastic rotation of the foundation. According to Grünberg and Göhlman, the static modulus of compressibility, $E_{s,stat}$, can be used instead of the dynamic modulus, Eq 2.10. [9].

$$c_{s,stat} = \frac{E_{s,stat}}{f' \cdot \sqrt{A_{foundation}}} \quad (2.10)$$

In subsection 2.4.5, an alternative approach is introduced to determine the subgrade modulus, called "spring stiffness". It is important to note that despite the different terminology, the concept of spring stiffness aligns with the subgrade modulus. Dividing the subgrade modulus by an area yields a "spring stiffness".

2.4.5 Stiffness

The stiffness of the foundation is determined by the strength and stiffness of the soil embedment. This modeling approach stems from the finite stiffness characteristic inherent in foundations. Because foundations have a limited ability to resist deformation, it's essential to adopt a modeling that reflects soil behavior as a non-rigid mass. It's common to use spring element boundary conditions to represent soil properties.

It's natural that the soil behaves in a nonlinear manner, meaning that foundation springs are modeled as nonlinear. The stiffness chosen is dependent on the strain level experienced for the specific load case being conditioned. A commonly referenced concept in discussions about soil mechanics is the shear modulus G . This modulus relates to the initial, G_0 as a function of the shear strain γ . To accurately validate the strains, please refer to [7], section 8.4 titled 'Foundation Stiffness'.

Table 2.5: Strain intervals most common for the Wind turbines.

Type of loading	Strain interval
Earthquake	$[10^{-2} - 10^{-1}]$
Wind and ocean waves	$[10^{-3} - 10^{-2}]$
Rotating machines	(10^{-5})

In table 2.5 the three most common sources of dynamic loading of soils are shown.

The selection of foundation spring stiffness depends on the assumed soil conditions and the mode of motion. The stiffness of the springs is determined based on the established values of the shear modulus, denoted as G , and the Poisson's ratio for

the soil. These values are referenced in Table 2.6. It is important to mention that these springs represents a static stiffness. The dynamic loading might deviate from this behaviour, especially in high frequency. However, according to DNV-RISØ the static stiffness of onshore wind turbines is sufficient for representing dynamic stiffness in structural analysis.

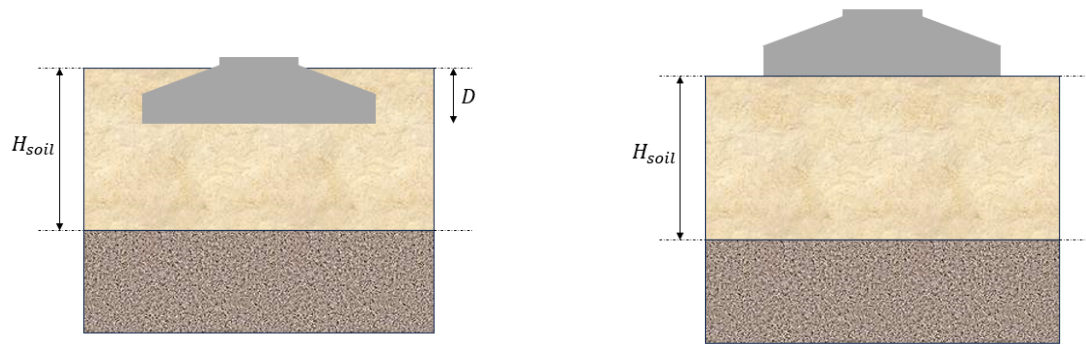
The table below distinguishes between foundations on soil on top of bedrock, left column, and on soil, right column. The variable H denotes the depth of the soil layer until another soil type is encountered, while R represents the foundation's radius. Another approach would be to fully account for a fully embedded foundation, Fig 2.7a. In that case Table 2.7 is utilized. Modeling the foundation directly on the soil without embedding yields a more conservative result, as it does not fully account for the soil's contribution to resisting horizontal loads, except the frictional forces.

Table 2.6: Spring stiffness equations of half space foundations.

Mode of motion	Foundation Stiffness on bedrock	Foundation Stiffness on soil
Vertical	$K_v = \frac{4GR}{1-\nu} \left(1 + 1.28 \frac{R}{H}\right)$	$K_V = \frac{4G_1R}{1-\nu_1} \left(\frac{1+1.28\frac{R}{H}}{1+1.28\frac{R}{H}\frac{G_1}{G_2}}\right); 1 \leq \frac{H}{R} \leq 5$
Horizontal	$K_H = \frac{4GR}{1-\nu} \left(1 + 1.28 \frac{R}{H}\right)$	$K_H = \frac{8G_1R}{1-\nu_1} \left(\frac{1+\frac{R}{2H}}{1+\frac{R}{2H}\frac{G_1}{G_2}}\right); 1 \leq \frac{H}{R} \leq 4$
Rocking	$K_R = \frac{8GR^3}{3(1-\nu)} \left(1 + \frac{R}{6H}\right)$	$K_R = \frac{8G_1R}{3(1-\nu_1)} \left(\frac{1+\frac{R}{6H}}{1+\frac{R}{6H}\frac{G_1}{G_2}}\right); 0.75 \leq \frac{H}{R} \leq 2$
Torsion	$K_T = \frac{16GR^3}{3}$	N.A

Table 2.7: Spring stiffness equations of embedded foundations.

Mode of motion	Foundation Stiffness
Vertical	$K_V = \frac{4GR}{1-\nu} \left(1 + 1.28 \frac{R}{H}\right) \left(1 + \frac{D}{2R}\right) \left(1 + (0.85 - 0.28\frac{D}{R}) \frac{D/H}{1-D/H}\right)$
Horizontal	$K_H = \frac{8GR}{1-\nu} \left(1 + \frac{R}{2H}\right) \left(1 + \frac{2D}{3R}\right) \left(1 + \frac{5D}{4H}\right)$
Rocking	$K_R = \frac{8GR^3}{3(1-\nu)} \left(1 + \frac{R}{6H}\right) \left(1 + 2\frac{D}{R}\right) \left(1 + 0.7\frac{D}{H}\right)$
Torsion	$K_T = \frac{16GR^3}{3} \left(1 + \frac{8D}{3R}\right)$



(a) Embedded case.

(b) Half space case.

Figure 2.7: Illustration of the two different cases.

2.5 Structural foundation design

In this section, the process of designing foundations for wind turbines will provide a broad overview of the various components involved in designing a foundation. First, an examination of the basic codes and standards that serve as guidelines will be undertaken. Subsequently, concrete design will be addressed, including the determination of necessary reinforcement and considerations regarding fatigue. Additionally, geotechnical factors will be discussed to ensure a comprehensive understanding.

2.5.1 Concrete

Concrete is a versatile construction material renowned for its durability and strength. Composed primarily of cement, water, and aggregates such as sand and gravel, concrete exhibits a remarkable combination of properties essential for various applications. Its compressive strength allows it to withstand heavy loads, making it ideal for building foundations. Due to its high density the concrete also work as a heavy weight for the wind turbine to prevent overturning. However, due to concrete's poor properties with tensile stresses, reinforcement is needed.

The foundation is subjected to shear forces, normal forces and moment. By using numerical methods it's possible to obtain section forces in the foundation, which is a necessity considering design of the reinforcement. In order to verify the concrete capacity, EN 1992-1-1:2005 can be utilized.

2.5.2 Reinforcement

The reinforcement is arranged symmetrically around the center of the foundation cage. Arrangement of the reinforcement begins at the bottom in both radial and tangential directions. Further, placement of top and shear reinforcement is then carried out.

To design the reinforcement, EN 1992-1-1:2005 can be applied. The forces subjected to the reinforcement are gained from the internal forces gathered from the FEM software

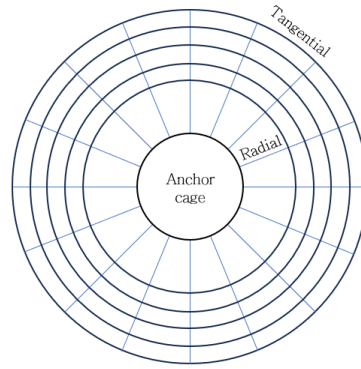


Figure 2.8: Illustration of the tangential and radial reinforcement.

results. The reinforcement is checked both in the radial direction and tangential direction both in the bottom and top part of the foundation.

In Plane Stresses

Normal forces per unit length in the x - and y - direction are denoted as N_x , N_y . The foundation will also be subjected to a shear force per unit length denoted as N_{xy} . If the sign convention of the force is positive it indicates that the normal force is tensile. The stresses are defined as the ratio of the normal force and the thickness, $\sigma_x = \frac{N_x}{t}$. The resistance of the reinforced concrete is sufficient if the normal forces is equal or less than the capacity of the combined steel and concrete.

A common concept when designing reinforcement is to consider the principal stresses. The principal stresses are associated with an inclined angle denoted as θ , with respect to the x -axis, where the shear forces are zero and solely normal forces active. The "principal plane" assumes that the shear resistance is ignored. [10] The concept is schematically shown in Fig 2.9a.

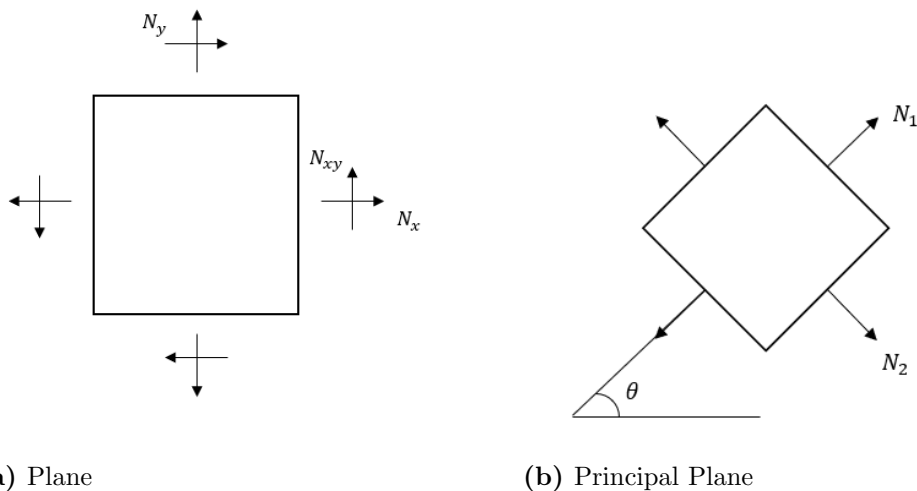


Figure 2.9: Illustration of the planes

The normal forces in the plane should be equal to the area of the reinforcement in the x - and y -direction, denoted as A_x , A_y times the resistance of the steel, denoted as f_x and f_y .

The reinforcement area is divided into to 4 different cases, suggested by EN 1992-1-1:2023 Annex G.

Case 1 : refers to the principal stresses, N_1 , N_2 both being in a compressive state and do not exceed the permissible compressive stress for uncracked concrete, f_{cd} . The case suggest that no reinforcement is needed and only the thickness of concrete will yield an optimal solution.

Case 2a, 2b: refers to that if the major principal force N_1 is tensile it is set to zero. Either no reinforcement is needed in the x -direction and the steel reaches permissible tensile stress in the y -direction, f_{yd} . Or the opposite case where no reinforcement is needed in the y -direction and the steel reaches permissible tensile stress in the x -direction, f_{xd} .

Case 3: refers to the areas of the reinforcement in both directions A_x , A_y being greater than zero and the resistance $f_y = f_x = f_d$.

The equations for each case are summarized in Table 2.8.

Table 2.8: Overview of the four different cases.

Case	Condition	Reinforcement and Forces
1	$\frac{N_x N_y}{N_{xy}^2} > 1$	$A_x = A_y = 0$
2a	$\frac{N_x}{ N_{xy} } < -1$ $\frac{N_x N_y}{N_{xy}^2} \leq 1$	$A_x = 0$ $A_y f_{yd} = N_y - \frac{N_{xy}^2}{N_x}$ $N_2 = N_x + N_y - A_y f_y$ $= N_x + \frac{N_{xy}^2}{N_x}$
2b	$\frac{N_y}{ N_{xy} } < -1$ $\frac{N_x N_y}{N_{xy}^2} \leq 1$	$A_y = 0$ $A_x f_{yd} = N_x - \frac{N_{xy}^2}{N_y}$ $N_2 = N_y + \frac{N_{xy}^2}{N_y}$
3	$\frac{N_x}{ N_{xy} } \geq -1$ $\frac{N_y}{ N_{xy} } \geq -1$	$A_x f_{yd} = N_x + N_{xy} $ $A_y f_{yd} = N_y + N_{xy} $ $N_2 = -2 N_{xy} $

Flexural Forces

The design of the reinforcement assumes the foundation as a concrete slab subjected to flexural forces. Although the equations used are not included in the EN 1992:2005, they do not conflict with the ISO clause regarding security treatment. The design criteria specified in the reference [10] can be adhered to, which include:

- $x_u/d < 0.25$, $f_{ck} < 50$ MPa or $x_u/d < 0.15$, $f_{ck} > 55$ MPa
- Steel class property with high ductility, B or C
- Ratio of moment at intermediate supports to the moments in the span should be between 0.5 and 2.0.

A concrete slab is subjected to three different moments. M_x and M_y represents bending moment about the x - and y -axis respectively. The twisting moment is denoted with M_{xy} . The required reinforcement to resist the flexural forces are divided into two categories, flexural steel required at the bottom denoted as M_{yu}^b , M_{xu}^b and flexural steel required at the top, M_{yu}^t , M_{xu}^t .

Table 2.9: Description of Conditions for Bottom and Top Reinforcement.

Position	Condition	Reinforcement Adjustment
Bottom	a) If $\frac{M_x}{ M_{xy} } \geq -1$ and $\frac{M_y}{ M_{xy} } \geq -1$	$M_{xu}^b = M_x + M_{xy} $ $M_{yu}^b = M_y + M_{xy} $
	b) If $\frac{M_x}{ M_{xy} } < -1$ and $M_y - \frac{M_{xy}^2}{ M_x } > 1$	$M_{xu}^b = 0$ $M_{yu}^b = M_y - \frac{M_{xy}^2}{M_x}$
	c) If $\frac{M_y}{ M_{xy} } < -1$ and $M_x - \frac{M_{xy}^2}{ M_y } > 1$	$M_{yu}^b = 0$ $M_{xu}^b = M_x - \frac{M_{xy}^2}{M_y}$
	d) If none of the above conditions are valid	$M_{xu}^b, M_{yu}^b = 0$
Top	a) If $\frac{M_x}{ M_{xy} } \leq -1$ and $\frac{M_y}{ M_{xy} } \leq 1$	$M_{xu}^t = M_x - M_{xy} $ $M_{yu}^t = M_y - M_{xy} $
	b) If $\frac{M_y}{ M_{xy} } > 1$ and $M_x - \frac{M_{xy}^2}{M_y} < 0$	$M_{yu}^t = 0$ $M_{xu}^t = M_x - \frac{M_{xy}^2}{M_y}$
	c) If $\frac{M_x}{ M_{xy} } > 1$ and $M_y - \frac{M_{xy}^2}{M_x} < 0$	$M_{xu}^t = 0$ $M_{yu}^t = M_y - \frac{M_{xy}^2}{M_x}$
	d) If none of the above conditions are valid	$M_{xu}^t, M_{yu}^t = 0$

Combined in plane and flexural Forces

The structural foundation design will however be influenced by a combination of in-plane forces, represented by N_x , N_y , and N_{xy} , along with the flexural forces mentioned earlier. Employing the sandwich model, Fig 2.10, one can accurately determine the necessary reinforcement for accommodating both in-plane and flexural forces. The Sandwich model is presented in the Eurocode 2- Part 2: Concrete Bridges- Design and detailing.

The calculations are carried out as the thickness being divided into two layers. Determination of the thickness corresponds to twice the distance from the outer layer to the center of the reinforcement. The denoting of y_s superior and y_i inferior is a

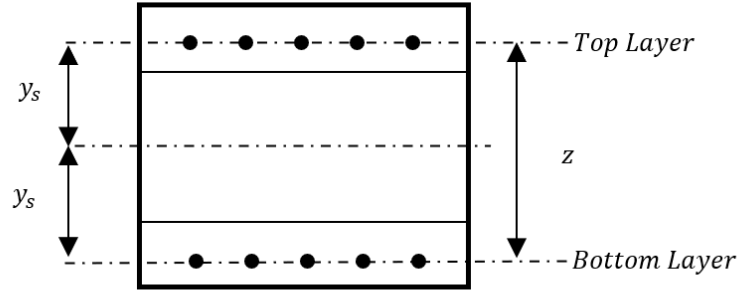


Figure 2.10: Illustration of the Sandwich model

representation of the distance top the centroidal axis, $z = y_s + y_i$. In addition, the normal forces are distributed between the upper and lower layers of reinforcement, denoted as N_s and N_i respectively. To ensure that the resultant force aligns with the centroidal axis, one can solve for N_s and N_i ,

$$N_s = N \left(1 - \frac{y_s}{z} \right)$$

$$N_i = N \left(1 - \frac{y_i}{z} \right)$$

Subjecting moment to the foundation can be replaced by corresponding couple forces by dividing the subjected moment with the leverage arm, $\pm M/z$. Total distributed force in respective layer can therefore be described as

$$N_s = N \left(1 - \frac{y_s}{z} \right) - \frac{M}{z},$$

$$N_i = N \left(1 - \frac{y_i}{z} \right) + \frac{M}{z}$$

Consideration must be given to the fact that the superior y_s and inferior y_i distances will differ due to the practical impossibility of laying reinforcements in the x and y directions within the same plane. To simplify calculations, it can be assumed that the distances are averaged between bottom and top reinforcement, ensuring computational efficiency without compromising on final result.

2.5.3 Shear reinforcement

The shear capacity can be checked for different stages, depending on the concrete condition. The first case refers to the shear capacity of the concrete exceeding the shear forces. For this case, no reinforcement is needed due to the concrete's capacity to withstand the shear force. The second case refers to a cracked concrete where shear reinforcement is needed.

The shear capacity of the concrete without reinforcement can be expressed according the empirical formula, Eq 3.24

$$V_{Rd,c} = \left[C_{Rd,c} k (100 \rho_{ck} f_{ck})^{\frac{1}{3}} + k_1 \sigma_{cp} \right] b_w d \geq [v_{min} + k_1 \sigma_{cp}] b_w d \quad (2.11)$$

If the shear force exceeds the concrete shear capacity shear reinforcement is needed. The resistance of shear is the smallest value of Eq. 2.12 and Eq. 2.13

$$V_{Rd,s} = \frac{A_{sv}}{s} \cdot z \cdot f_{ywd} \cdot \cot \theta \quad (2.12)$$

$$V_{Rd,max} = a_{cw} \cdot b_w z \cdot \nu_1 \cdot f_{cd} \cdot \frac{1}{\cot \theta + \tan \theta} \quad (2.13)$$

The parameters are referenced in annex C.

Punching

Punching shear failure is a result of high loads or reaction forces acting on a small surface. Punching consideration is a must for concrete slabs that are supported by columns. The failure refers to that a column have enough capacity to withstand the load from the slab but the shear forces exceeds the capacity of the slab. As a results the concrete slab gets punched through by the column, Fig 3.7.

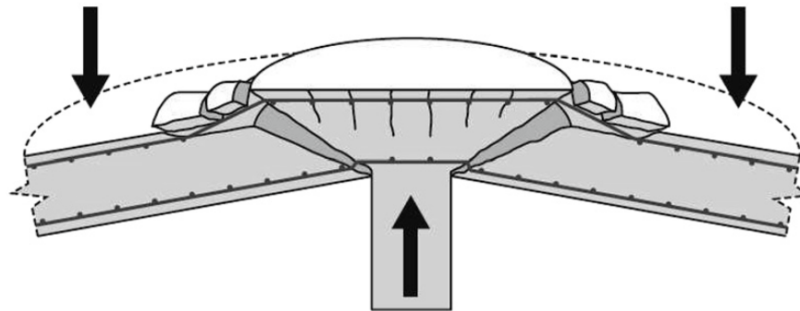


Figure 2.11: Punching shear failure of slab (Pollack Periodica 2021).

The SS-EN 1992-1-1:2005, 6.4 provide the general rules for punching. Although it's a simplification of the real action it is always a conservative approach. This was confirmed by, Scharda et al., 2018, in their paper on punching shear failure of concrete slabs. As a result they found that the Eurocode provided a theoretical punching shear value of 60.13 kN, while measurments of mean values from testing gave a value of 177.42 kN. Further, modeling simulations provided similar results to that of the real measured ones. [11]

Wind turbine foundations can in a similar way be checked for punching. The attachment of the tower to the anchor cage imposes significant local forces on the foundation. Therefore, it is essential to verify the punching capacity of this critical region.

2.5.4 Fatigue

The common term fatigue is a technical term used to describe how cyclic loads may cause a complete failure in a material after time. When components are subjected to cyclic loading microscopical cracks appear, which are of irreversible type. The cracks are not noticeable with the naked eye and will eventually propagate into a larger crack. This can lead to the hazardous effect of a sudden brittle failure even for a ductile material as steel. Most common fatigue checks are performed on welds which are usually subjected to higher eigenstresses. Wind turbines are structures that are subjected to one of the highest number of loading cycles of any structures, hence verification of fatigue control is of high importance.

The cyclic loading manifest itself in the material changing properties. Results show that with increasing number of loading cycles the tensile plot shifts to higher stress values. This means that resistance of material is increased with increasing number of cycles. The reason for this is that to reach plastic strain, higher stresses are required [12]. This saturation of the material can be exploited when designing for fatigue by ensuring that the load cycles can extend to the saturated behaviour.

Fatigue according to RISØ [7], can be verified in a simpler manner if the stress spectrum is: $\Delta\sigma_s \leq |70|$ MPa. In the case of higher stress variations more sophisticated fatigue analysis has to be used in order to guarantee structural integrity. In that case fatigue verification can be carried out using Markov's matrices. In combination with the Palmgren-Miners rule damage accumulations, D_d , being less than one insures fatigue verification.

$$D_d = \sum_i^n \frac{n_i}{N_{fi}} < 1 \quad (2.14)$$

n_{Ei} number of cycles measured within a certain stress range
 N_{fi} Number of cycles to failure

According to J. J. Kauzlarich [13], the Palmgren-Miner rule simplifies the assessment of fatigue life by not considering prior stress history or the sequence of loadings. Kauzlarich explains, "The PM rule does not take into account prior stress history or sequence of loadings so that when applying the rule to gross cycles with few load changes it can be highly inaccurate, with the summation varying all the way from 0.18 to 23. However, if the various load amplitude cycles are mixed in a quasi-random manner the summation tends to approach unity at the time of failure".

The EN 1993-1-9 : 2005, provide fatigue load parameters and verification formats using the Palmgren-Miner rule too. The annex provide guidelines how to evaluate cycle counting, stress spectrum range, cycles to failure and verification formats.

The subsequent section is a direct reproduction of the EN 1993-1-9:2005 to outline methods that could potentially be utilized.

- **Cycling counting**

Stress histories may be evaluated by either of following counting methods:

- rain-flow method
- reservoir method

to determine

- stress ranges and their numbers of cycles
- mean stresses, where the mean stress influence needs to be taken into account.

- **Stress spectrum**

- 1) The stress range spectrum should be determined by presenting the stress ranges and the associated number of cycles in descending order.
- 2) Stress range spectra may be modified by neglecting peak values of stress ranges representing less than 1 % of the total damage and small stress ranges below the cut off limit.

- **Cycles to failure**

The damage during it's life is calculated from

$$D_d = \sum_i^n \frac{n_{Ei}}{N_{Ri}} \quad (2.15)$$

where

n_{Ei} is the number of cycles associated with the stress range $\gamma_{Ff}\Delta\sigma_i$ for band in the factored spectrum

N_{Ri} is the cycles obtained from factored $\frac{\Delta\sigma_C}{\gamma_{Mf}} = N_R$ for stress range of γ_{Ff} .

- **Verification**

The fatigue assessment should satisfy the following criteria, whether it is based on damage accumulation or stress range.

$$D_d \leq 1$$

or

$$\gamma_{Ff}\Delta\sigma_{E,2} \leq \sqrt[3]{D_d} \frac{\Delta\sigma_c}{\gamma_{Mf}}$$

2.5.5 Fatigue Estimation methods

There are different fatigue estimation methods. The most common methods are sub-categorized into:

- Counting methods
- Frequency domain or spectral methods
- Stochastic methods

- Hysteresis operator

All cases assumes that the input is obtained from time history of the loading parameter [12].

SN Curve

Commonly used in Fatigue assesment is the SN curve. The graph corresponds to a downward sloping curve that depicts the relation between stress amplitudes $\Delta\sigma$ and number of cycles to failure N_f . The curve represent the the maximum stress level to cycles a speciemen can manage before failure. The SN curve is divided into three subareas: plastic region where low cycle fatigue appears, elastic region where high cycle fatigue appears and the infinite life area.

Naturally it is not feasible to obtain a Wöhler curve, commonly named as the S-N curve, for outside laboratory objects. In order to do so, a linear model can be fit to the S-N data. The model is formulated by the *Basquin expression* $\sigma_a = \sigma'_f(2N_f)^b$.

The SN curve is useful to decide whether a component can manage the stress levels with respect to the number of cycles it's subjected to. Combining a stress history, SN Curve and the Palmgren-Miner rule to describe the cumulative damage, one can perform a fatigue verification.

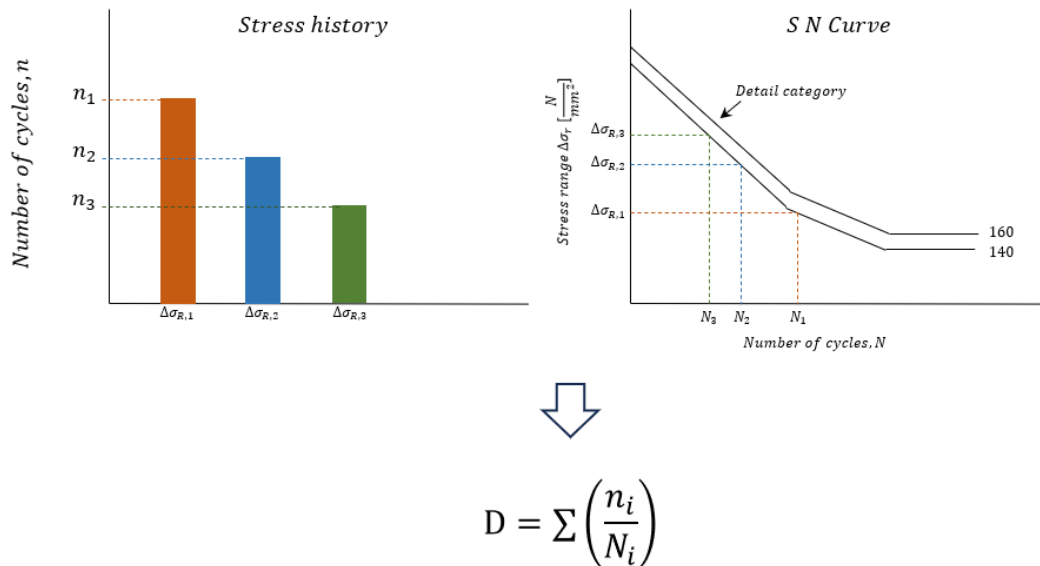


Figure 2.12: Illustration of fatigue verification using the Palmgren-Miner rule

Counting methods

Cycle counting methods are algorithmic methods that are based on combining fatigue cycles from maxima and minima within cycle. Together with damage accumulations

rules, such as Palmgren-Miner, one can perform a fatigue assessment. The Palmgren-Miner rule is simple due to its linear representation of damage accumulation. Applying it assumes a fixed load, hence neglecting interactions that effect contribution to the damage, in random loading [14]. There are several versions of the counting method such as, peak valley counting, levelcrossing counting and reservoir counting. These different counting methods are different from one another depending on how a cycle is being defined and counted for. The most accurate in identifying the damaging effects caused by complex loading is the Rainflow Counting method, (RFC)[15]. For future examination and comparison between the counting models reference to [16] and [17] is recommended. The Rainflow Counting method involves having a structural model, stress range history with cycles, rainflow count of the history, and a damage accumulation rule.

Today there are toolboxes used to gather output from amplitudes and cycle mean histograms from simulations which can be conformed into a Rainflow Matrix (RFM).

The RFM is constructed by discretizing a load signal into a chosen number of bins. Each bin contains load cycle means and amplitudes, which are summarized into a *Rainflow Matrix*. Next part will provide a more detailed explanation.

Rainflow counting

The Rainflow counting uses the definitions of a rainflow cycle, which means that a local maximum of load is paired with a particular minimum one. The minimum, m_i is a representation of the smallest deviation to the maximum, M_i defined as the rainflow cycle starting at M_i .

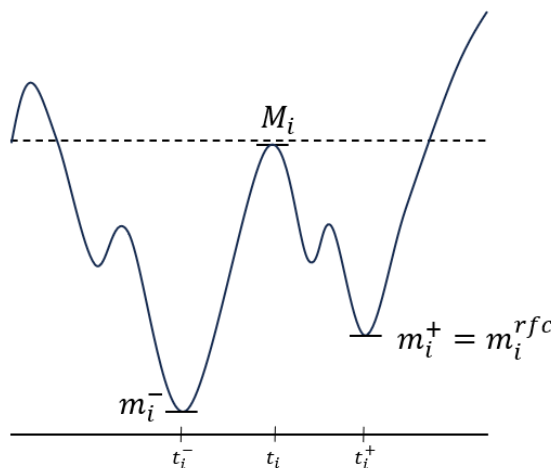


Figure 2.13: Illustration of how a rainflow cycle is defined

Introducing a load function dependent on t denoted as $L(t)$, where M_i is a local maxima occurring at time t_i . Further we have a representation of, the local minima, m_i for time. The sequence we get from a certain time, t_i is denoted with (m_i, M_i) and is called the sequence of *turning points*. Another necessary term used is the min-to-max count

(mM) which is a set of the sequence (m_i, M_i) . The (mM) count can be described with bivariate histograms called Markov matrices [18].

The simplified introduction to the mathematical rain flow method can then be combined with the commonly used Palmgren-Miners rule, mentioned earlier, to evaluate the total damage accumulated from the arbitrary load function $L(t)$.

$$D = \sum_i^n f(m_i^{rfc}, M_i) \quad (2.16)$$

where

f is the damage function caused for one cycle, which is defined in, [18].

$$f(\sigma_k, \sigma_l) = c(\sigma_k - \sigma_l)^\beta \quad (2.17)$$

where

β, c are material constants obtained from constant amplitude experiments.

In simpler terms, the approach involves using simulated or experimental loading data which lacks a particular pattern and projecting this onto a graph displaying amplitudes and the occurrence of these amplitudes, 2.14. By utilizing *Hysteresis filtering*; removing cycles whose contribution to the total damage is insignificant and *Peak-valley filtering*; preserving only the max and min values of the cycles, one is provided with simpler more manageable data.

Rainflow counting, available through toolboxes in various programs, filters stress history data into cycles n_i and stress ranges σ_i from the stress history curve that do not contribute to damage accumulation. This process ensures that the oscillations remain within the hysteresis curve. Depending on cycle definition such as, the four consecutive stress points, S1, S2, S3, S4 one define the inner stresses and outer stresses. If the inner stress range is bounded by the outer stress range a cycle is counted. For the opposite case it is not counted. This is put into a rainflow matrix and evaluated along the stress curve. As mentioned there are toolboxes for rainflow counting methods, which returns cycle counts and stress ranges from load input based on the ASTM E 1049 standard [19].

Depending on the threshold of the bins, the peak values are corrected into, one can achieve varied constellations of inner and outer stress levels. Naturally the more bins you have the greater amount of unique values you have, hence also a larger matrix. In Figure, 2.15 it is shown that the values of 5 and 3, corresponding to an inner stress range is counted as one cycle into the rainflow matrix.

The rainflow matrix can be combined with the Wöhler curve mentioned previously and in combination with Palmgren-Miners rule fatigue assesment can be performed.

Rainflow Histogram

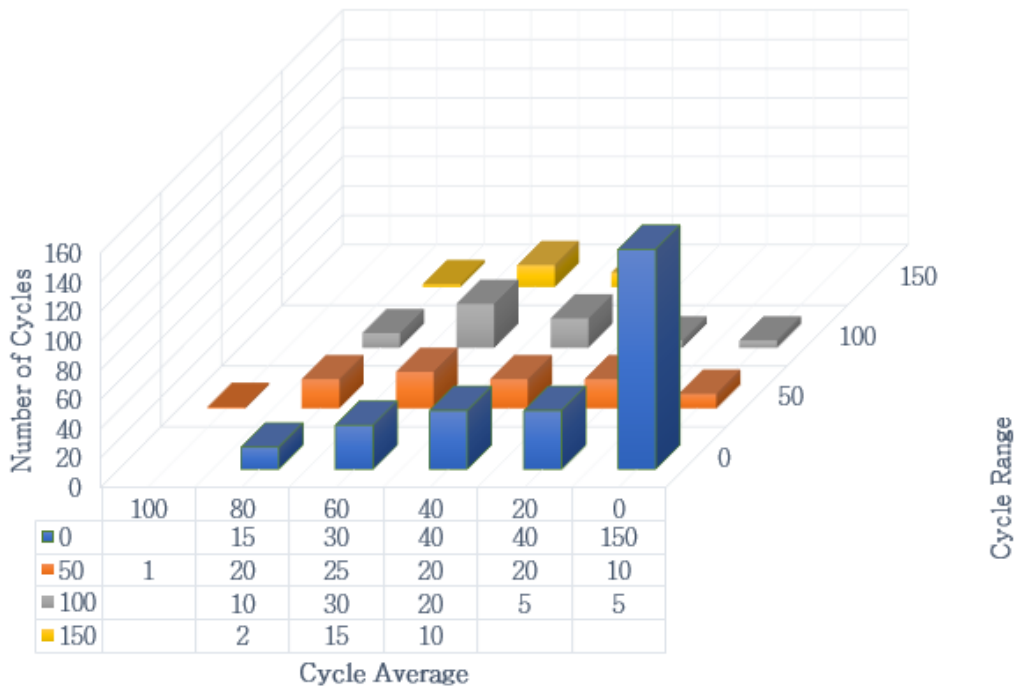


Figure 2.14: Illustration of filtered data plotted in histogram. The values in the figure are intended to illustrate how the data might appear.

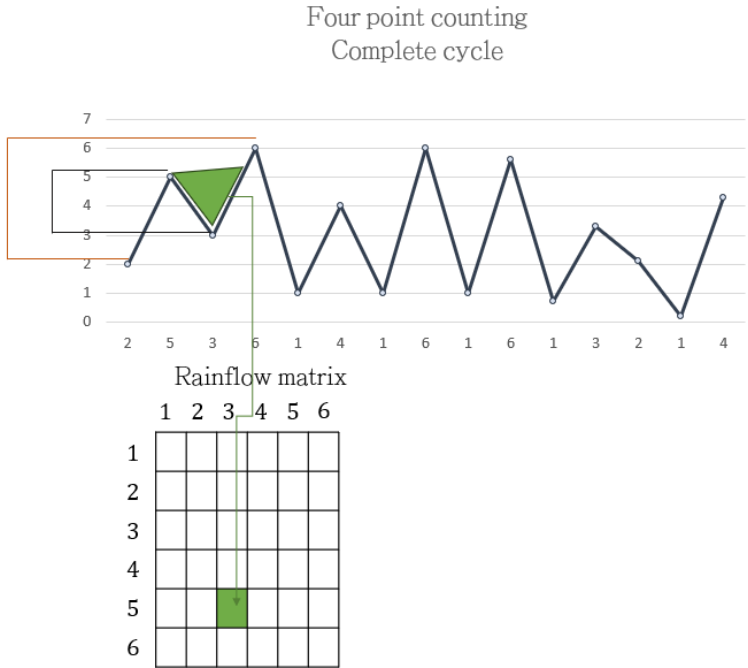


Figure 2.15: Demonstration of four point counting with 6 bins

2.5.6 Crack width

The concrete foundation will be influenced from loads, temperature and concrete shrinkage which will generate cracks. The crack width, w , needs to be checked according to DS411 (DS411, 1999) in order to guarantee structural integrity, Eq 2.18.

$$w = 5 \cdot 10^{-2} \cdot \sigma_s \sqrt{a_w} \quad \text{mm} \quad (2.18)$$

The crackwidth parameter, a_w is calculated from the active concrete area, A_{cef} and the sum of critical width diameter of the reinforcement, denoted as d_w .

$$a_w = \frac{A_{cef}}{d_w} \quad (2.19)$$

The stresses in the reinforcement, σ_s , is assumed to take all of the tension load, hence assuming concrete take no loads in the tension zone. This is a conservative evaluation, however it guarantees structural reliability.

In a broader context, these calculations are influenced by additional factors such as temperature and shrinkage. While it is feasible to simulate these behaviors, they will not be addressed further. Instead, a general guideline according to DSV-482 (1999) is referenced to. Generally, crack width should fall within the range of [0.2, 0.3] mm. To not mitigate further cracking, it is recommended that temperatures do not exceed 70°C, a concern typically not encountered in wind turbine foundation design. However, cross section temperature differences remain a significant consideration. The temperature difference, ΔT , across the cross-section should therefore not exceed 15°C to prevent excessive cracking.

2.6 Modeling foundations

For specialized foundations, like those necessary for wind turbines, relying solely on analytical calculations is inadequate for ensuring an effective and sustainable design. By modeling the foundation with computational heavy numerical solver programs, such as SAP 2000 a more detailed, more optimal and correct result can be achieved, e.i if the model is correct.

In this thesis the modeling will be generated automatically from an API script to SAP2000. The script outputs section moments, shear forces and normal forces that later will be used to design reinforcement or change the geometry for a more optimal solution based on the literature above.

2.6.1 Finite element method

The Finite element method, FEM, is a numerical method used for solving differential equations. It's used in analysis of structures, heat transfer, fluid flow, mass transport

and even electromagnetic potentials. When designing a foundation or any type of structure in detail the method provides highly accurate results, i.e if it is used correctly.

Today several FEM programs are offered and the heavy calculations are being performed automatically. However, the understanding of how different factors affect the output of the solutions makes it vital to understand how it works in order to save time and guarantee accurate results.

The FEM software's offers different kinds of elements such as frame- , shell- and solid elements etc, all of which have different pros and cons. Solid elements which represents three-dimensional volumes are suitable for modeling solid structures subjected to complex loading, such as foundation. However, solid elements are highly time consuming.

Shell element

Shell elements are used to model structures in which the thickness is smaller than other dimensions, i.e thin walled structures such as plates and shells. Shells can be defined in several ways. Importantly to know is the conventional shells which have displacement and rotational degrees of freedom. In contrast there is continuum shell elements where the thickness is determined from the element nodal geometry. These only consider displacement degrees of freedom. The shells are defined with a mid surface of the thickness assigned to it meaning that if the shell is subjected to bending the middle will always remain of the same length.

The reference plane can be placed freely within the thickness of the shell element. This flexibility allows for more precise modeling of different structural behaviours. The bending results are influenced by this chosen plane, and the membrane actions are inherently linked to it, ensuring an accurate representation of both in-plane and out-of-plane deformations. [20]

The conclusion is that the placement of the reference plane influences the bending behavior of shell elements, which in turn affects the overall analysis results.

3 Methods used in the scripting

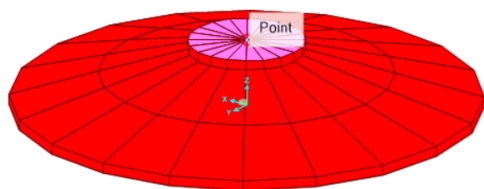
This chapter outlines the automated design process generated within the API script. The arrangement of these subchapters mirrors the coding sequence, facilitating the reader’s comprehension of the program’s structure. Certain details are omitted here and instead referenced in the Annex to maintain a broader perspective and avoid excessive equation-focused discussions. This chapter serves as a guide for interpreting the verification and calculation results generated by the script, providing a comprehensive overview.

3.1 FE-Modelling

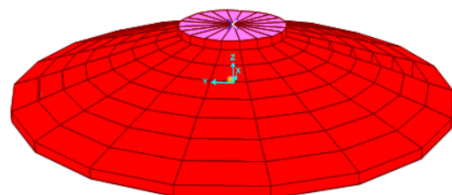
The foundation geometry was modeled with four node shell area elements for the concrete foundation and three node elements for the concrete pedestal in the SAP 2000 software. The shell thickness was assigned to the area elements to replicate the slope property of the wind turbine foundation. The function for offsetting the area elements was created so that the slope of the foundation got calculated by using simple trigonometry and then later divided into the number of circles provided by the user. The function then automatically creates a list of offsets and assigns the offset to respective group.

The elements were organized into two groups where the first group corresponded to each circle group labeled as Group 1, 2.. i, depending on the amount of circles the user chose to input, Fig 4.5. The other group, called the "Cakegroup 1,2 ... i", corresponds to that of a cake slice and is dependent on the user’s choice of number of points per circle.

Figure 3.1 represent a model of the same foundation but with two different defined



(a) Model of foundation where three circles are defined by the user. The point represents an offset point where the load was applied.



(b) Model of foundation where eight circles are defined by the user.

Figure 3.1: Comparison of the same foundation with a more refined mesh to the right.

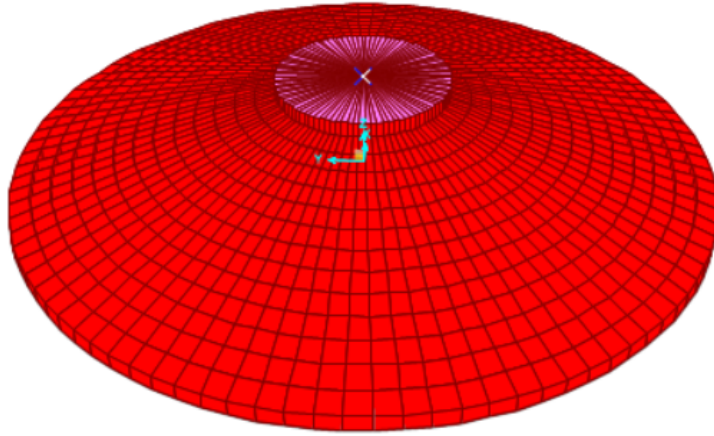


Figure 3.2: Model of foundation where fourteen circles and 100 number of points per circle are defined by the user. The load was assigned to the center point.

parameters for *number of circles* by the user. Fig 3.1a is defined with three circles while 5.2b represents a defined number of eight circles. As shown, the mesh becomes more refined as the user define a higher number of circles. A further parameter with the name *number of points per circle* was added so that the user can specify how many points should be defined for each circle. Fig 3.2 showcase an exaggerated amount of points per circle set to 100 by the user and fourteen circles.

It's essential to understand that although each area element appears to be resembling a solid element, it's not to be mistaken for a solid element. In the model the calculations are still carried out on thick shell area elements.

Meshing

The meshing of the foundation was created so that the user easily enough can change it by assigning either more points to the circles or more circles, described in section 3.1. A convergence study of the meshing is presented in 4.6. Meshing of the pedestal (inner most circle) has been simplified with only three noded elements, but will be further revised with a new version.

Loads

A point was offset at the same height as the maximum height of the foundation to the center point, see Fig 3.2. The pedestal was assumed rigid; hence, the pedestal nodes were constrained to the offset point, creating a rigid body. This rigid body is an assumption due to the high stiffness and anchoring in the anchor cage. Loads provided by the manufacturer were then assigned to the offset center point accordingly:

$$Load_{ULS} = [N_x, N_y, N_z, M_{xx}, M_{yy}, M_{zz}]$$

To simulate the soil's weight to the foundation load, each area element was assigned with a uniform downward directed load. The magnitude was determined by multiplying the assumed bulk density for soil, $\rho_{soil} = 1500 \text{ kN/m}^3$, by the height of the soil above the area element. Because of the foundation's sloped geometry, the load increase linearly as the distance from the foundation center increases. Due to SAP2000 not being able to handle linear area loads, a uniform load per area group was created. However, in order to be on the safe side, the height of the soil above the foundation model was set to the mean value of the inclined points of the area element, so that the magnitude of the uniform load resembles that of a linear one, while still being constant over the the area element group, Fig 3.3.

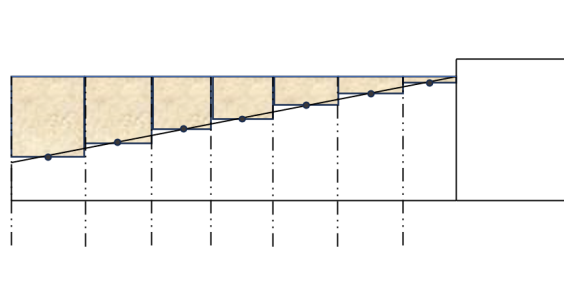


Figure 3.3: Illustration of soil assumed soil height.

The loads were further categorized into different load cases, Favourable ULS (Ultimate Limit State), SLS (Serviceability Limit State), FLS (Fatigue Limit State) and unfavourable ULS, each with different or same safety factor. Each load case was defined as static nonlinear, Fig 3.4.

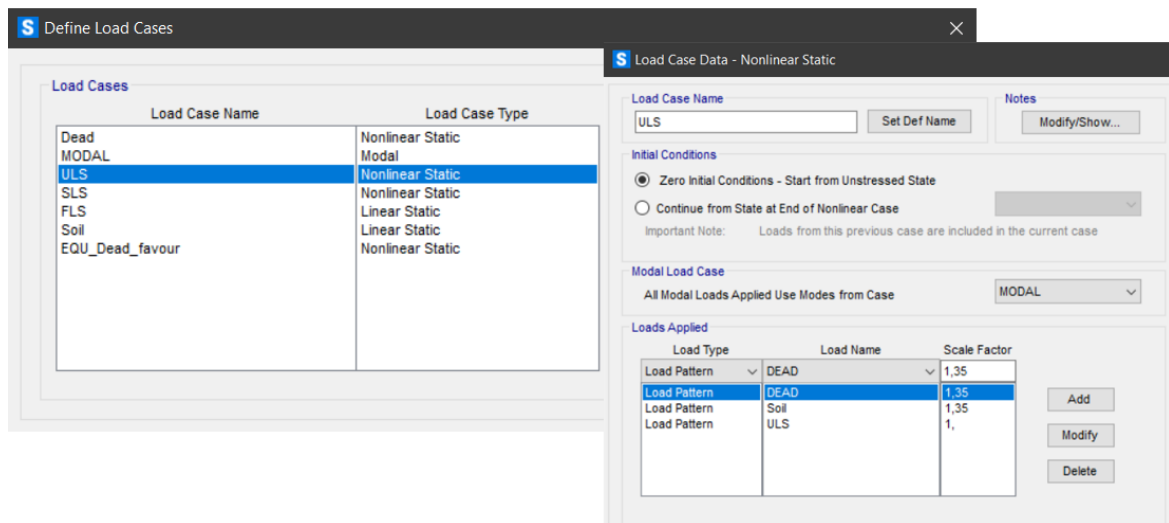


Figure 3.4: Setting of ULS.

Restraints and Constraints

Springs were added to the area elements in the vertical direction at the bottom face of the foundation model. These springs were assigned with the feature of only accepting compression to replicate soil-like behavior when loading the foundation vertically. Additionally, springs were assigned to the area elements to the horizontal local axis, capable of accepting both compression and tension. The local coordinate system was set to be pointing inwards to the center point. By incorporating horizontal and vertical springs, the foundation ensures stable boundary conditions.

The stiffness of the springs in the horizontal, K_H , and vertical direction, K_V was determined according to Equations 3.1 and 3.2, respectively. The values of the stiffnesses were defined based on the expressions provided in Table 2.6. For convenience, the same equations are repeated below.

$$K_V = \frac{4G_1R}{1 - \nu_1} \left(\frac{1 + 1.28\frac{R}{H}}{1 + 1.28\frac{R}{H}\frac{G_1}{G_2}} \right); \quad 1 \leq \frac{H}{R} \leq 5 \quad (3.1)$$

$$K_H = \frac{8G_1R}{1 - \nu_1} \left(\frac{1 + \frac{R}{2H}}{1 + \frac{R}{2H}\frac{G_1}{G_2}} \right); \quad 1 \leq \frac{H}{R} \leq 4 \quad (3.2)$$

These equations determine the stiffness of the vertical and horizontal springs based on the ratio of the height, H to the radius, R of the springs, as well as material properties, G_1, G_2, ν_1 .

Another approach following J.Grünberg's, Concrete structures for wind turbine (2013) was also carried out by assuming a dynamic modulus of elasticity, $E_{s,dyn}$ and a static modulus of elasticity, $E_{s,stat}$. The dynamic and static foundation modulus was then calculated according Eq. 3.3 and 3.4. The moduli were then assigned to the spring stiffness of the model.

$$c_{s,dyn} = \frac{E_{s,dyn}}{f' \cdot \sqrt{A_{foundation}}} \quad (3.3)$$

$$c_{s,stat} = \frac{E_{s,stat}}{f' \cdot \sqrt{A_{foundation}}} \quad (3.4)$$

3.2 Verifications and model estimates

This section details the process of verifying rough estimates of the overturning control, bearing capacity of soil, and sliding capacity. The subchapters follow a consistent format aligning with the script.

Given the extensive number of equations involved, only key components are highlighted to facilitate comprehension. This approach aims to offer a clearer insight into the output of the script which will further be displayed in section 4.3.

3.2.1 Soil bearing capacity in drained conditions

The designing bearing capacity for drained conditions was carried out according to DNV-RISØ, described in section 2.4.2.

$$q_{ult} = c' N_c b_c s_c i_c + p_0 N_q b_q s_q i_q + \frac{1}{2} \gamma' b'_{eff} N_\gamma b_\gamma s_\gamma i_\gamma \quad (3.5)$$

Further the effective Area, A_{eff} was calculated with the formula:

$$A_{eff} = \left(2 \cdot \left(\frac{D}{2} \right)^2 \cdot \cos \left(\frac{e}{\frac{D}{2}} \right) - e \cdot \sqrt{\left(\frac{D}{2} \right)^2 - e^2} \right) \quad (3.6)$$

where

D is the diameter of the foundation

The major axes, l_e and b_e for circular shapes, Fig 2.6 was calculated according:

$$l_e = 2 \cdot \frac{D}{2} \sqrt{1 - \left(1 - \frac{b_e}{2 \frac{D}{2}} \right)} \quad (3.7)$$

$$b_e = \max \left(2 \cdot \left(\frac{D}{2} - e \right), W' - 2 \cdot e_{W'} \right) \quad (3.8)$$

where:

W' is the foundation width which is set to 0 if foundation is circular
 $e_{W'}$ the eccentricity of the load for width.

The total resistance of the foundation, R_{Rd} , was determined using the ultimate bearing capacity, q_{ult} , and the effective area, A_{eff} :

$$R_{Rd} = q_{ult} \cdot A_{eff} \quad (3.9)$$

This resistance was verified to ensure structural safety, under the condition that it should exceed the applied vertical load V_{Ed} :

$$R_{Rd} \geq V_{Ed} \quad (3.10)$$

The utilization of the bearing capacity, denoted $utilization_{bearingcapacity}$, was then calculated as the ratio of the applied vertical load to the total resistance of the foundation:

$$utilization_{bearingcapacity} = \frac{V_{Ed}}{R_{Rd}} \quad (3.11)$$

Note that the method described herein is presented briefly, as it encompasses a multitude of parameters. For a comprehensive understanding, it is recommended to read the DNV-RISØ "Guidelines for Design of Wind Turbines", which are based on EN-standards. The method has been integrated into the script to enable the autonomous generation of tables and verification procedures.

3.2.2 Sliding capacity

The sliding capacity was determined accordingly:

First the friction angle was defined:

$$\mu = \tan(\phi') \quad (3.12)$$

Then the sliding capacity was determined.

$$R_k = A_{eff} \cdot c_{eff} + V_{Ed} \cdot \mu \quad (3.13)$$

Lastly, verification and utilization was performed:

$$\text{Control : } R_k \cdot 0.4 \geq H'_{Ed} \quad (3.14)$$

$$\text{Utilization : } utilization_{sliding} = \frac{H'_{Ed}}{R_k \cdot 0.4} \quad (3.15)$$

where

H'_{Ed} equivalent horizontal force.

V_{Ed} Design vertical load from superstructure.

3.2.3 Overturning Control

To ensure stability against overturning, a process in six steps following the guidelines outlined in DNV-RISØ is given below .

1. Determination of Compressed Area (A_{comp}) :

The compressed area, A_{comp} , was initially calculated. This calculation involved dividing the applied vertical load, V_{Ed} , by the allowable design stress, σ_{allow} , obtained from geotechnical studies. In this thesis, it is assumed that $\sigma_{allow} = 400$ MPa.

$$A_{comp} = \frac{V_{Ed}}{\sigma_{allow}} \quad (3.16)$$

2. Calculation of Height of Compressed Segment (h_{comp}):

To determine the lever arm (e_d), the height of the compressed segment (h_{comp}) was calculated using Eq. 3.17. This equation considers the angle of the compressed segment, θ_{comp} , which represents the inclination of the compressed segment of the foundation and the diameter of the foundation, D' .

$$h_{comp} = \frac{D'}{2} - \frac{\cos \theta_{comp}}{2} \cdot \frac{D'}{2} \quad (3.17)$$

3. Angle Calculation (θ_{comp}):

The angle of the compressed segment, θ_{comp} , was determined. It played a crucial role in the estimation of the compressed area.

$$A_{comp} = \frac{\theta_{comp} - \sin \theta_{comp}}{2} \cdot \left(\frac{D'}{2}\right)^2 \quad (3.18)$$

4. Calculation of the lever arm (e_d):

Once h_{comp} and θ_{comp} were known, the lever arm, e_d , was calculated using the diameter of the foundation and the height of the compressed segment.

$$e_d = \frac{D'}{2} - \frac{h_{comp}}{2} \quad (3.19)$$

5. Determination of Stabilizing Moment (M_{stb}):

The stabilization moment, M_{stb} , was calculated using A_{comp} and e_d , which are crucial parameters in the calculation to verify the overturn verifications.

$$M_{stb} = A_{comp} \cdot \sigma_{allow} \cdot e_d \quad (3.20)$$

6. Verification and Utilization:

Finally, the calculated stabilizing moment, M_{stb} , was compared to the design bending moment, M_{Ed} . The utilization factor, $utilization_{overturning}$, was determined to assess stability against overturning.

$$M_{stb} \geq M_{Ed} \quad (3.21)$$

$$utilization_{overturning} = \frac{M_{Ed}}{M_{stb}} \quad (3.22)$$

These steps verify that the wind turbine foundation remain stable and can resist overturning under applied loads.

3.3 Reinforcement Design

This section outlines the methodology used to design reinforcement based on the results obtained from the finite element analysis performed in SAP 2000. It aims to offer insight in what equations has been implemented into the script in order to design the reinforcement automatically. Consider the chapter as an introduction to how the script uses output from the FEM analysis and outputs required reinforcement area in the radial, tangential, and vertical direction.

3.3.1 Combined in plane and flexural bending reinforcement

The sandwich model discussed in section 2.5.2 served as the foundation for reinforcement design. However, slight modifications were made to accommodate the slope of the foundation. The superior, y_s and inferior y_i distances, corresponding to the thickness of the area element experiencing the highest maximum or minimum value of forces was determined. This involved calculating the distances by assuming a centroidal axis for the thickness of the area element. To facilitate a clear understanding, the design concept has been divided into three faces.

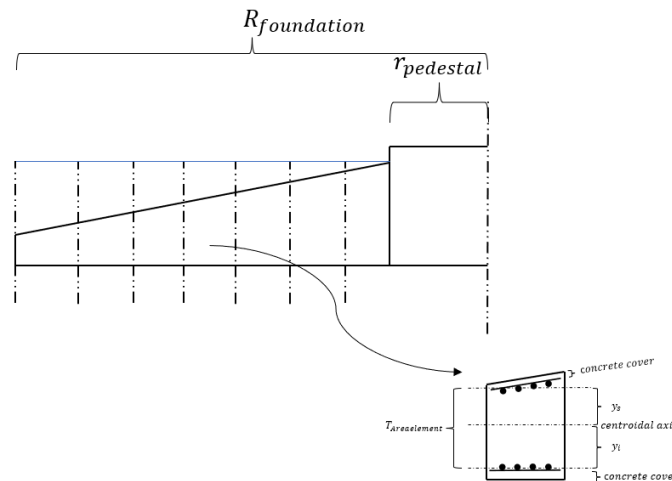


Figure 3.5: Illustration of how the superior and inferior distance was determined from particular a area element.

Firstly, the thickness of both the top and bottom layers was determined using Equation 3.23:

$$z = \langle T_{Araelemnt} \rangle - (d_{conc} + d_{top} + d_{bottom}) \quad (3.23)$$

where

d_{conc} is the concrete cover

d_{top} diameter of the top reinforcement

d_{bottom} diameter of the bottom reinforcement

$\langle T_{Araelemnt} \rangle$ mean thickness of the area element thickness

Next, the inferior and superior distances were determined by defining the centroidal axis of the area element subjected to designing section forces. The superior distance, y_s , is defined as the average height of the two inclined points of the area element thickness, as illustrated in Figure 5.2a.

Finally, the in-plane forces for the bottom and top reinforcement layers were computed. This involved calculating:

$$\begin{aligned} \frac{M_x}{z} & \quad [\text{N/mm}] \\ \frac{M_y}{z} & \quad [\text{N/mm}] \\ \frac{M_{xy}}{z} & \quad [\text{N/mm}] \\ N_x \left(1 - \frac{y_s}{z}\right) & = N_x \left(1 - \frac{y_i}{z}\right) \quad [\text{N/mm}] \\ N_y \left(1 - \frac{y_s}{z}\right) & = N_y \left(1 - \frac{y_i}{z}\right) \quad [\text{N/mm}] \\ N_{xy} \left(1 - \frac{y_s}{z}\right) & = N_{xy} \left(1 - \frac{y_i}{z}\right) \quad [\text{N/mm}] \end{aligned}$$

The design process proceeded according to the category under which it fell, as referenced in section 2.5.2. The diameter and the steel class of the reinforcement was defined, see Chapter 4 for definition.

$$\begin{aligned} A_x f_{yd} & = N_x + |N_{xy}|, & A_x & \quad [\text{mm}^2/\text{mm}] \\ A_y f_{yd} & = N_y + |N_{xy}|, & A_y & \quad [\text{mm}^2/\text{mm}] \end{aligned}$$

where

A_k reinforcement area
 f_{yd} design yield stress of reinforcement

An example of such a design process for a slab is presented by P. Bhatt and T. J. MacGinley in Reinforced Concrete Design to Eurocode, Annex D.

3.3.2 Shear Reinforcement

The shear reinforcement was designed to withstand the designing shear force V_{Ed} . In other words $V_{Ed} < V_{Rd}$. The designing shear force V_{Ed} was provided from the FEM analysis. In order to minimize the shear reinforcement, shear reinforcement was only added in the critical zones. The critical zone refers to the area where the concrete is not sufficient to withstand the shear force and therefore needs the support by reinforcement. In order to find critical zones the shear resistance of the concrete foundation was determined in all groups, Fig 3.6. The sections that were investigated are dependent

on the users' input on how many circles one wants to add to the foundation model. In Fig 3.6 number of circles refers to the dashed lines.

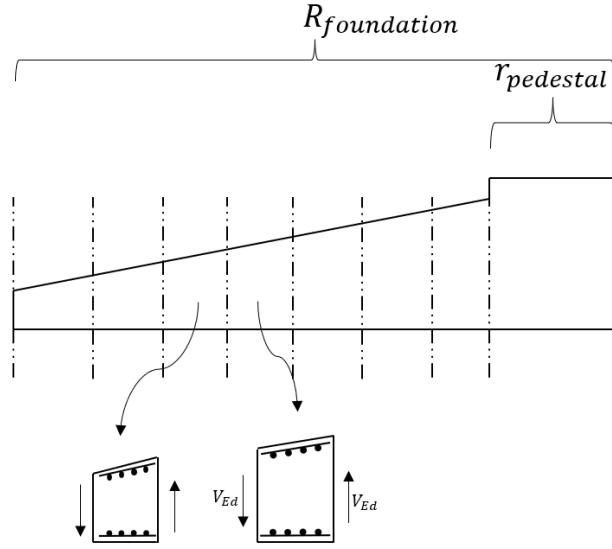


Figure 3.6: Sections where designing shear forces are evaluated and compared to the shear resistance of the concrete. Number of circles has been put to eight for illustrative purposes.

In the section where the shear resistance for concrete without rebars falls short of the designing shear force , $V_{Rd,c} < V_{Ed}$, shear reinforcement was added and designed for. The process involved:

Step 1 Calculate shear resistance without shear reinforcement for the concrete in defined sections of the foundation Eq. 3.24.

$$V_{Rd,c} = \left[C_{Rd,c} k (100 \rho_{ck} f_{ck})^{\frac{1}{3}} + k_1 \sigma_{cp} \right] b_w d \geq [v_{min} + k_1 \sigma_{cp}] b_w d \quad (3.24)$$

Step 2 Determine in what region $V_{Rd,c} < V_{Ed}$.

Step 3 Add defined shear reinforcement to the critical area with a specified c/c distance

Step 4* Calculate shear resistance now with shear reinforcement added to the concrete.

Step 5 Optimize until requirement is satisfied $V_{Rd, shearconc} > V_{Ed}$.

Step 4* The shear resistance with added reinforcement was calculated according to SS-EN 1992-1-1:2005; where lowest values of 3.25 and 3.26 were taken.

$$V_{Rd,cs} = \frac{A_{sw}}{s} z f_{ywd} \cot \theta \Leftrightarrow \frac{A_{sw}}{s} = \frac{V_{Rd,cs}}{z f_{ywd} \cot \theta} \quad (3.25)$$

$$V_{Rd,max} = \alpha_{cw} b_w \nu_1 \frac{f_{cd}}{\cot \theta + \tan \theta} \quad (3.26)$$

where

s Spacing of the stirrups

A_{sw} Cross-sectional area of the shear reinforcement

f_{ywd} Design yield strength of the shear reinforcement

ν_1 Strength reduction factor for concrete cracked in shear

α_{cw} Coefficient taking account of the state of the stress in the compression chord

Special notes and considerations are referred to in Annex C.

Note that this method only accounts for straight shear reinforcement and not inclined.

3.3.3 Punching

The punching verification followed SS-EN 1993-1-1:2005 section 6.4. The design was made so that V_{Ed} did not exceed the design value of the punching shear resistance **without** punching shear reinforcement, $V_{RD,c}$ or the value of punching shear resistance **with** punching shear reinforcement, $V_{RD,cs}$. In other words depending upon if shear punching reinforcement is needed the design was made to which $V_{Ed} < V_{Rd,max}$.

The basic control perimeter u_1 was regarded as two times the effective depth, $2d$ from the loaded area. Note that depth, d for objects with variable depths may be assumed to be the depth to the loaded area, according to SS-EN 1992:2005, Fig 3.7.

The support reaction was assumed eccentric with respect to the control perimeter, which yields the expression for maximum shear stress, Eq 3.27

$$V_{Ed} = \beta \frac{V_{Ed}}{u_i d} \quad (3.27)$$

d is the mean effective depth of the slab, which may be taken as $(d_y + d_z)/2$

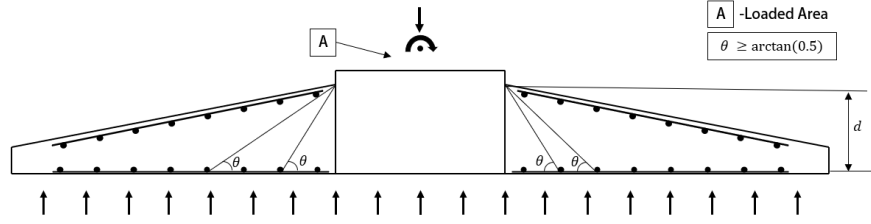
d_y, d_z is the effective depths in the y - and z - directions of the control section

u_i is the length of the control perimeter being considered

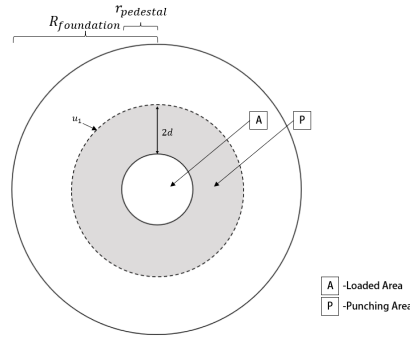
$$\beta = 1 + 0.6\pi \frac{e}{D + 4d} \quad \text{for circular heads}$$

Details are described in Annex C, according to SS-EN 1992:2005.

Considerations regarding the load within the control perimeter that adds resistance to the structural system were subtracted when designing the punching shear force. That is, the load within the punching area pointing in the opposite direction 3.7b was subtracted from the total shear force of the design, V_{Ed} .



(a) Illustration of the foundation with reinforcement in bottom and top edges. Effective depth is denoted with d .



(b) Illustration of the possible punching area from a bird view.

Figure 3.7: Illustrations of the foundation and possible punching area.

3.4 Fatigue

The fatigue verification process utilized Markov matrices, as detailed in section ???. Initially, data was collected from wind turbine manufacturers, who conducted the rainflow counting analysis for the moment ranges and their corresponding cycle counts.

Subsequently, results were obtained from the fatigue load case, using a reference load, $M_x = 1$ kNm. From the results of this dataset, the maximum stress in a reinforcement element under the fatigue load case, denoted as σ_s , was extracted. The maximum stress was then scaled by the ratio of the data collected measured moment to the reference moment 1 kNm, yielding σ_R . Utilizing the S-N curve and the defined detail category, the corresponding number of cycles to failure was determined for the particular stress range.

Damage calculation ensued from dividing the measured number of cycles for a given moment by the number of cycles to failure. Cumulative damage, denoted as D , was derived by summing up all individual damages. Verification of fatigue was established by comparing the cumulative damage D to 1. If $D < 1$, the fatigue is verified and structure deemed safe.

To summarize:

1. Rainflow counted data with moment ranges and their corresponding cycles, was obtained from the manufacturer.
2. Maximum stress, σ_s , was extracted from the FEM model.

3. σ_s was then multiplied by the ratio of moment range to reference moment to obtain σ_R .
4. Utilizing the S-N curve, the number of cycles to failure was determined for each stress range.
5. The cumulative damage, D was determined by summing the ratio of cycles for each moment range to the corresponding number of cycles until failure,
$$D = \sum_1^i \frac{n_i}{N_{f,i}}$$
6. Fatigue verification was established by ensuring $D < 1$.

Table 3.1 presents a graphical overview of the process. The values are not to be construed as actual results or real values; rather, they serve as clarification. To aid in the interpretation of the table, reference to Figure 2.12 is recommended.

Table 3.1: Overview of the fatigue verification.

Moment range [Nm]	Cycles, n	$\Delta\sigma_R$ [MPa]	Cycles to failure, N	Damage $\frac{n}{N}$
500	5000	$\frac{500}{1000} \cdot \sigma_s$	N_1	d_1
750	400	$\frac{750}{1000} \cdot \sigma_s$	N_2	d_2
1000	30	$\frac{1000}{1000} \cdot \sigma_s$	N_3	d_3
		...		
Cumulative damage				$D = \sum d_i$

4 Results

This chapter outlines the parameters defined and the results that were output from the script. The defined parameters were gathered from comparable wind turbine cases. The parameters can easily be adjusted in the automated script if one wants to investigate other types of geometries, materials, reinforcement, soils and loads.

The flowchart replicates the scripts process of handling the parameters and outputs the result. It provides an understanding of how it operates.

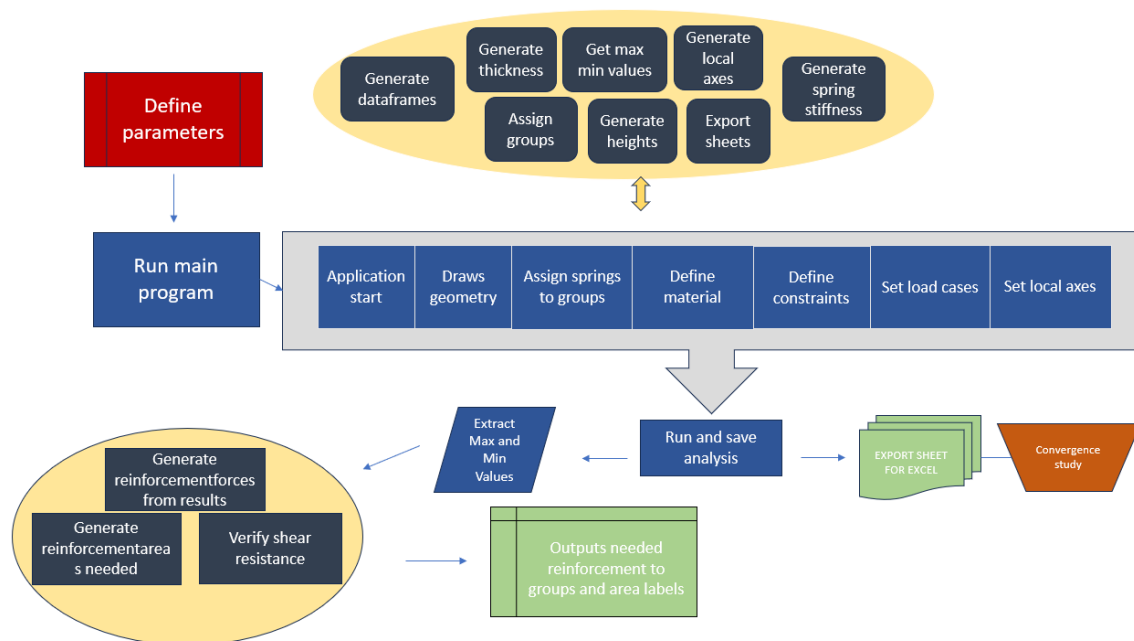


Figure 4.1: Flowchart of how the script works and utilize the results to design reinforcement.

4.1 Definitions

Subsequent section aims to define the parameters which were used for the design of the wind turbine foundation. The table includes definitions used for the modeling and FEM calculation, which generates the required reinforcement area for the foundation in the tangential and radial directions. The table is complemented with more definitions for the calculations regarding the bearing capacity, overturning capacity, and sliding capacity.

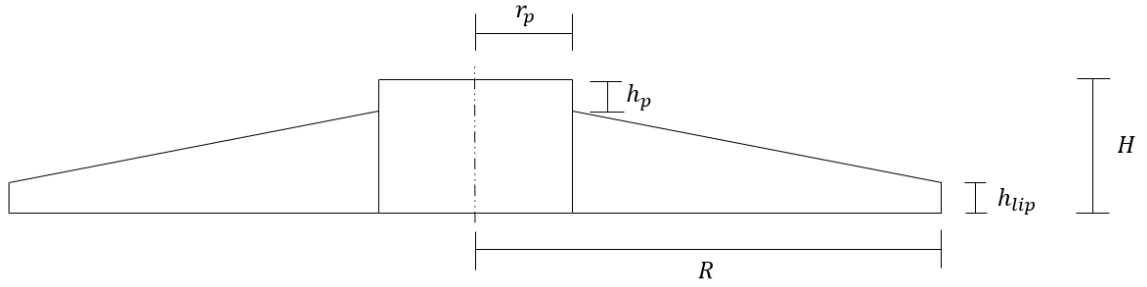


Figure 4.2: View of the geometry parameters.

Table 4.1: Defined parameters for the examined foundation.

Variable	Value	Unit	Description
Geometry			
R	12	m	Radius of the foundation
H	3.5	m	Height of the foundation
h_p	0.5	m	Pedestal height
h_{lip}	0.5	m	Height of the lip
r_p	3	m	Pedestal radius
Concrete and Steel Classes			
Concrete	C35/45	-	Concrete class
f_{ck}	45	MPa	Characteristic compressive strength of concrete
γ_c	1.5	-	Partial safety factor for concrete
f_{sk}	500	MPa	Characteristic yield strength of reinforcement
γ_s	1.15	-	Partial safety factor for reinforcement
f_{yd}	435	MPa	Design yield strength of reinforcement
c_{nom}	40	mm	Nominal cover
d_{top}	20	mm	Diameter of top reinforcement
d_{bot}	20	mm	Diameter of bottom reinforcement
Loads			
M_x	771	kN	Moment about the x-axis
M_y	225750	kN	Moment about the y-axis
M_z	9585	kN	Moment about the z-axis
F_x	1727	kN	Force along the x-axis
F_y	-27	kN	Force along the y-axis
F_z	-7742	kN	Force along the z-axis
ρ	1500	kg/m ³	Density
Soil Bulk Density	14.7	kN/m ³	Bulk density of soil

4.2 Spring stiffness

The stiffness of the vertical and horizontal spring is a built in function in the script and follows the equation structure of Table 2.6 or 2.7 and Fig 2.7 depending on what case one would like to investigate. In this thesis, the spring stiffness was determined for an embedded foundation.

Table 4.2: Defined parameters for determining the spring stiffness for embedded foundation.

Variable	Value	Unit	Description
R	12	m	Radius of the foundation
H_{soil}	30	m	Height of the soil to second layer
G_1	180	MPa	Shear modulus of the first soil layer
G_2	540	MPa	Shear modulus of the second soil layer
ν_1	0.3	-	Poisson ratio for dense sand
D	3	m	Depth of burial

$$K_V = \frac{4GR}{1-v} \left(1 + 1.28 \frac{R}{H}\right) \left(1 + \frac{D}{2R}\right) \left(1 + \left(0.85 - 0.28 \frac{D}{R}\right) \frac{D/H}{1 - D/H}\right) = 25350 \text{ kN/m}^3$$

$$K_H = \frac{8GR}{1-v} \left(1 + \frac{R}{2H}\right) \left(1 + \frac{2D}{3R}\right) \left(1 + \frac{5D}{4H}\right) = 38880 \text{ kN/m}^3$$

4.3 Bearing capacity

The analysis of bearing capacity was performed using a separate script from the main one. This study provided a preliminary indication of the soil's capacity to withhold the foundation for drained condition. The tables present the same output as the script and will give an error if the total resistance for drained condition is not OK. In that case the foundation geometry should be changed before running the main script to do FEM-analysis.

Table 4.3: Defined parameters to verify the bearing capacity.

Variable	Value	Description
ϕ_k	38°	Characteristic friction angle
c	0	Characteristic cohesion (kPa)
α	0	The inclination of the foundation base to the horizontal
L_f	0	Foundation Length (circular foundation)
W_f	0	Foundation Width (circular foundation)
slope	0.02	Slope
$\gamma_{surcharge}$	18	Soil unit weight for surcharge calculation (kN/m ³)
γ_G	0.9	Partial Safety factor
σ_{allow}	400	Design load bearing capacity (kPa)

Table 4.4: Results of the bearing capacity.

Variable	Value	Unit	Description
$Volume_{concrete}$	673.73	m ³	Concrete foundation Volume
$Volume_{soil}$	816.04	m ³	Soil fill volume on top of foundation
e	3.58	m	Eccentricity of the load
A	452.39	m ²	Foundation Area
l_e	20.11	m	Major axis length for circular shape foundations
b_e	16.85	m	Major axis width for circular shape foundations
A_{eff}	234.33	m ²	Effective area
q_{ult}	958.49	kPa	Design bearing resistance of drained condition
R_{Rd}	224605.99	kN	Total resistance for drained condition
	OK	-	Control
	16.08%	%	Utilization

4.4 Sliding capacity

The analysis of sliding capacity was performed using the same script as for the one with bearing capacity. This study provided a preliminary indication if foundation sliding is at risk. The table present the same output as the script and will give an error if the criterion isn't fulfilled. In that case the foundation geometry should be changed before running the main script to do FEM-analysis.

Table 4.5: Results of the foundations sliding capacity.

Variable	Value	Units	Description
μ	0.5596	rad	Friction angle
H_{Ed}	1821.65	kN	Equivalent horizontal force
R_k	20213.62	kN	Sliding capacity
$R_k \cdot 0.4 > H_{Ed}$	OK	-	Control of sliding
	22.53%	%	Utilization

4.5 Overturning capacity

The analysis of overturning capacity was performed using the same script as for bearing capacity and sliding capacity. This provides an output for the foundation's stability. If the stabilizing moment is less than designing bending moment the script will output an error and the geometry should be changed before running the main script to do FEM-analysis.

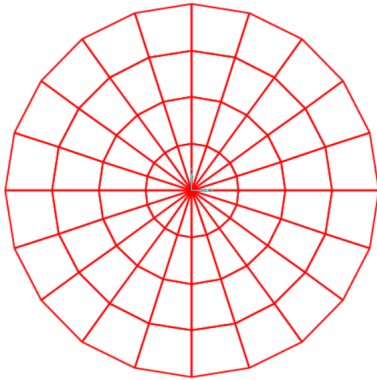
Table 4.6: Results of the foundation overturning capacity.

Variable	Value	Units	Description
A_{comp}	90.3061	m	Compressed area
θ_{comp}	2.1116	rad	angle of compressed segment
α_{comp}	20.8869	m	Width of the compressed area
h_{comp}	6.0894	m	Height of the compressed area
M_{stb}	323486.65	kNm	Stabilizing
M_{Ed}	231134.03	kNm	Design bending moment
	OK	-	Control for overturning
	71.45%	%	Utilization

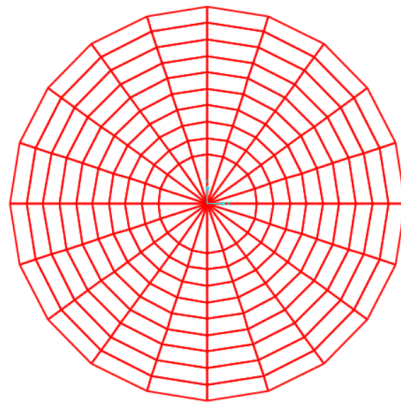
4.6 Convergence study

A convergence study was carried out to determine the most suitable mesh size. It is imperative to balance between computational efficiency and the accuracy of the results. While a finer mesh may yield marginally different results, the substantial increase in computational cost makes it impractical. Therefore, the aim of this study is to identify an optimal mesh size that ensures accurate results while minimizing computational resources.

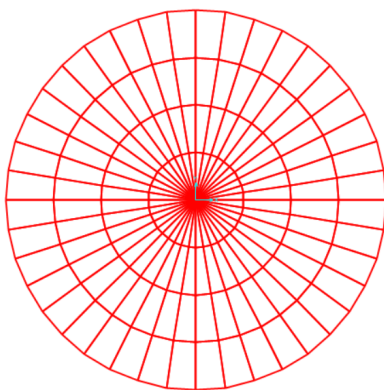
As described in section 3, the mesh size depends on the user's input of "number of points per circle" and "number of circles". The former determines the number of (x, y) coordinates generated to create one circle, while the latter defines the number of circles from the maximum radius to the innermost radius of the circle (pedestal radius). To provide a better understanding of this concept, Figure 4.3 illustrates various inputs used to define the mesh size.



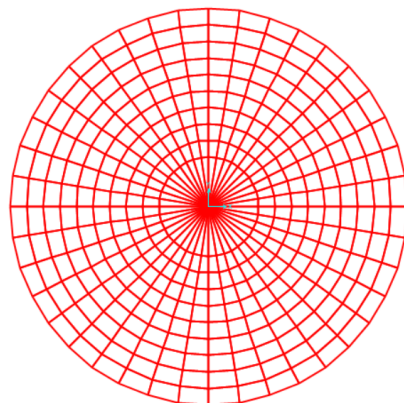
(a) 20 Number of Points 4 Number of circles.



(b) 20 Number of Points 10 Number of circles.



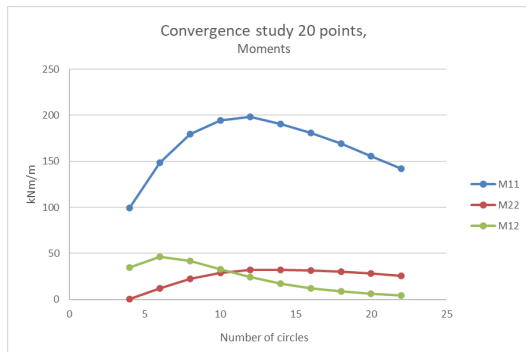
(c) 40 Number of Points 4 Number of circles.



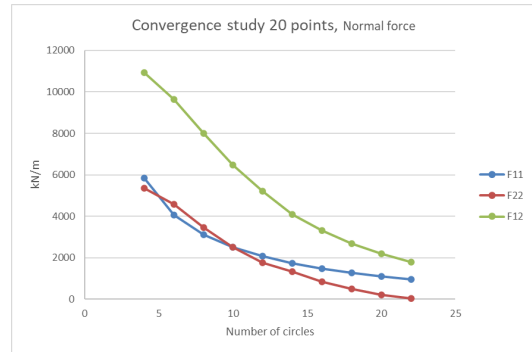
(d) 40 Number of Points 10 Number of circles.

Figure 4.3: Illustration of the mesh size definition.

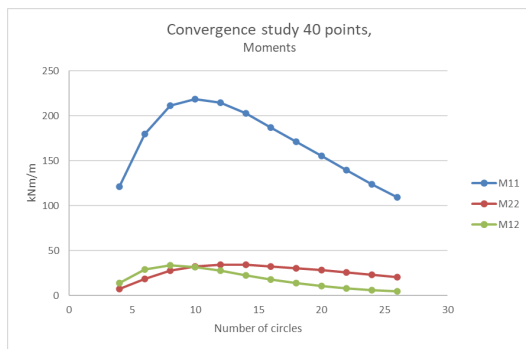
The results used for the convergence study refer to the section normal forces and moments in the plane of the area elements. The result of the forces was plotted against the mesh size.



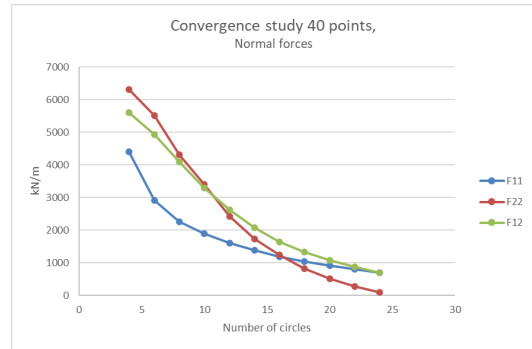
(a) Results for moments when 20 points per circle was applied.



(b) Results for normal forces when 20 points per circle was applied.



(c) Results for moments when 40 points per circle was applied.



(d) Results for normal forces when 40 points per circle was applied.

Figure 4.4: Convergence study of normal forces and moments. Indexing of M11, M22, M12, V13 refers to the direction of M_x , M_y , M_{xy} , V_{xz} .

4.7 Moments and Normal forces

This sections outlines the results gathered from running the script. The program will output and save dataframes from the FEM software SAP200. The feature of saving it in dataframes enables the user to easily sort out desired information from the result.

The maximum and minimum forces of M_{xx} , M_{yy} , M_{xy} , F_{xx} , F_{yy} , F_{xy} , V_{xz} , V_{yz} and the corresponding to the max and min forces were extracted, Table 4.7 and 4.8.

The AreaLabel column in Table 4.7 and 4.8 refers to the name that the software SAP2000 labels a specific area element in the model. An inconvenience if one uses a refined mesh due to the high number of labeling. In Table 4.9, however, the column, Area group is assigned by the script and corresponds to the group of the outermost circle (Group 1) to the innermost circle (Group 19).

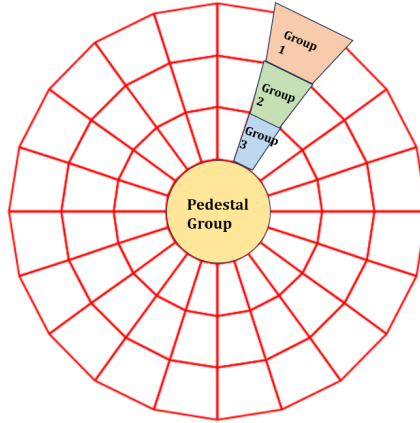


Figure 4.5: Group categorization with four number of circles, generate four groups in total. Groups 1, 2, and 3 constitute one category, forming a cake group.

Table 4.7: Max Values in ULS and corresponding forces to the max value. Marked value corresponds to the maximum.

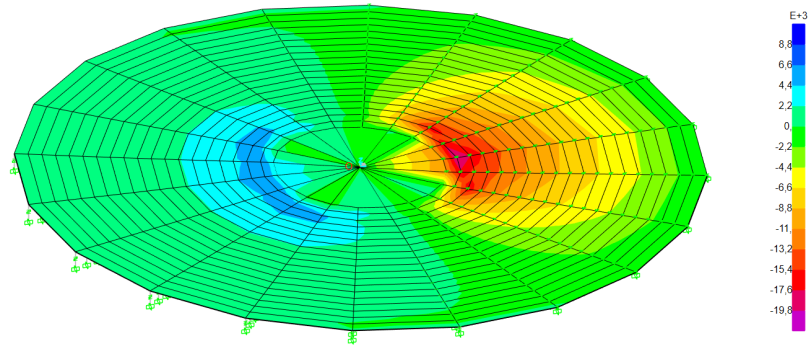
AreaLabel	OutputCase	F11	F22	F12	M11	M22	M12	V13	V23
348	ULS	9920.88	2457.58	5903.13	-42.06	-5.29	5.58	-174.38	192.47
347	ULS	7185.09	5578.83	5596.75	38.57	10.00	-5.07	-132.09	104.67
348	ULS	2160.34	905.47	6174.76	-37.18	-7.35	-7.65	-174.38	192.47
393	ULS	-1742.95	3466.30	-59.93	3950.03	-1802.59	-2012.65	513.57	1206.94
392	ULS	-250.30	4128.34	2554.83	242.96	4613.27	-7304.72	258.71	1346.30
392	ULS	-988.09	834.05	2970.16	849.83	1941.71	4657.74	258.71	1346.30
40	ULS	-1564.18	1784.96	1649.09	155.05	25.37	7.01	584.99	-14.54
400	ULS	-1195.69	-1741.30	-2328.50	-3549.34	-852.21	-6997.66	-86.50	2498.97

Table 4.8: Min Values in ULS and corresponding forces to the min value. Marked value corresponds to the min.

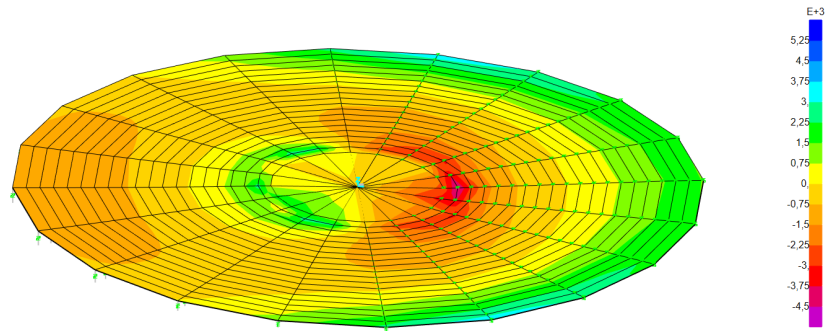
AreaLabel	OutputCase	F11	F22	F12	M11	M22	M12	V13	V23
361	ULS	-20665.89	-4676.59	485.65	55.63	11.91	12.18	214.04	382.40
344	ULS	-10060.58	-5067.02	3437.08	-47.00	-9.02	-6.10	145.53	193.10
353	ULS	2304.07	933.95	-5845.22	-37.27	-6.83	7.52	-173.75	-143.45
399	ULS	-1031.98	-3270.92	3275.75	-5117.40	-501.06	-4145.49	-340.18	427.22
400	ULS	-1305.65	-1763.30	-2606.19	-820.28	-7912.24	-7008.90	-86.50	2498.97
392	ULS	-250.30	4128.34	2554.83	242.96	4613.27	-7304.72	258.71	1346.30
398	ULS	859.59	-3845.85	1517.57	-5028.25	521.48	-364.62	-488.71	630.74
380	ULS	-20564.39	-4661.59	-890.43	36.54	10.46	13.65	215.04	-330.17

The results for the maximum and minimum section forces for the load cases are output by the script. The full result is presented in annex E.

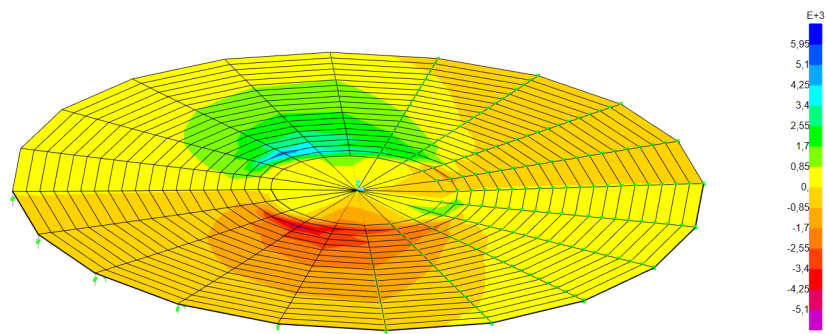
More illustrative results are shown in Fig. 4.6. The figure showcase the sectional normal forces corresponding to Table 4.7 and 4.8.



(a) Ultimate limit state load case for F11 element forces.



(b) Ultimate limit state load case for F22 element forces.



(c) Ultimate limit state load case for F12 element forces.

Figure 4.6: Normal section forces of the foundation area element. Negative values denote compression, while positive values indicate tension.

4.8 Tangential and radial reinforcement

The calculation of the reinforcement needed was carried out for all groups and subsequently organized according to the maximum area requirement for each specific group. During the analysis, both the maximum and the minimum values are examined. In order to have an optimized reinforcement design, the reinforcement arrangement should follow Table 4.9 which corresponds to the minimal required reinforcement area per millimeter.

Table 4.9: Designing reinforcement required categorized into groups.

Area group	Ax_{top}	Ay_{top}	Ax_{bottom}	Ay_{bottom}	Unit
Group1	1.19	3.95	1.26	4.18	(mm ² /mm)
Group2	0.67	4.16	0.73	4.11	.
Group3	0.97	3.31	1.02	3.58	.
Group4	1.36	2.76	1.39	2.78	.
Group5	1.73	2.41	1.77	2.39	.
Group6	2.14	2.11	2.21	2.09	.
Group7	2.57	1.83	2.61	1.82	.
Group8	3.04	1.64	3.10	1.63	.
Group9	3.50	1.67	3.52	1.67	.
Group10	4.05	1.68	4.10	1.68	.
Group11	4.54	1.81	4.55	1.80	.
Group12	5.24	1.95	5.29	1.96	.
Group13	6.06	2.34	6.11	2.35	.
Group14	7.01	2.92	7.05	2.93	.
Group15	8.39	3.72	8.44	3.73	.
Group16	9.95	5.05	9.99	5.05	.
Group17	13.16	7.34	13.21	7.35	.
Group18	18.22	9.61	18.16	9.61	.
Group19	11.46	13.41	11.45	10.20	.

4.8.1 Shear Reinforcement

The shear reinforcement is output by the script. First the script extracts the designing shear forces, V_{xz} , V_{yz} and calculates the concrete's capacity without reinforcement. The program outputs True if reinforcement is needed for that specific area element, Table 4.10. Further, the script saves the dataframe and computes the shear reinforcement needed for each group according Eq. 3.26, presented in table 4.11. Assumed value for $\cot \theta = 2.5$, according to Eurocode which recommend a value of, $1 \leq \cot \theta \leq 2.5$.

Table 4.10: Evaluating shear capacity of the concrete to examine if shear reinforcement is needed within the specific area element.

V_{Rd} (kN/m)	$V_{Ed,xz}$ (kN/m)	$V_{Ed,yz}$ (kN/m)	Area Label	Group	Reinforcement Needed
71.28	418.41	8.83	1	Group1	True
64.57	583.82	13.29	21	Group2	True
59.52	582.33	14.44	41	Group3	True
55.28	556.60	14.51	61	Group4	True
...

It is important to note that the group named *PedestalGroup* refers to the pedestal itself. This value should not be taken too seriously due to the script not accounting for the anchor cage. However, it is a good verification that the designing shear force is highest close to the pedestal group.

Table 4.11: Summary of design values and required shear reinforcement to each group.

Group	$V_{Ed,xz}$ (kN/m)	$V_{Ed,yz}$ (kN/m)	$\frac{A_{swxz}}{s}$	$\frac{A_{swyz}}{s}$	z (m)
Group1	419.24	37.23	1.54	0.14	0.25
Group2	584.99	53.65	1.70	0.16	0.32
Group3	583.50	58.25	1.41	0.14	0.38
Group4	557.74	62.13	1.15	0.13	0.45
Group5	529.14	66.77	0.95	0.12	0.51
Group6	502.29	70.54	0.80	0.11	0.58
Group7	478.05	73.71	0.68	0.11	0.64
Group8	455.68	75.79	0.59	0.10	0.71
Group9	435.43	77.56	0.52	0.09	0.78
Group10	417.06	79.16	0.46	0.09	0.84
Group11	397.43	79.91	0.40	0.08	0.91
Group12	380.14	87.41	0.36	0.08	0.97
Group13	367.52	96.74	0.33	0.09	1.04
Group14	361.09	109.01	0.30	0.09	1.11
Group15	361.81	125.02	0.28	0.10	1.17
Group16	371.67	147.47	0.28	0.11	1.24
Group17	394.05	174.62	0.28	0.12	1.30
Group18	443.37	267.80	0.30	0.18	1.37
Group19	215.04	382.40	0.14	0.25	1.43
PedestalGroup	513.57	2498.97	0.31	1.53	1.50

4.8.2 Punching

The results from checking against punching, according to section 3.27 indicate that the punching shear force is much less than the values from table 4.11. Hence no extra reinforcement is needed for punching.

Table 4.12: Summary of punching design forces.

Group	$V_{punching,xz}$ (kN/m)
Group1	45.13
Group2	62.98
Group3	62.82
Group4	60.04
Group5	56.96
Group6	54.07
Group7	51.46
Group8	49.06
Group9	46.88
Group10	44.90
Group11	42.79
Group12	40.92
Group13	39.57
Group14	38.87
Group15	38.95
Group16	40.01
Group17	42.42
Group18	47.73
Group19	23.15
PedestalGroup	55.29

4.9 Fatigue

This section outlines the results for fatigue verification. The script calculates the stresses in the reinforcement for the FLS load case after required reinforcement area was determined, Table 4.9.

The maximum stress, highlighted with gray in Table 4.13 is governing for fatigue verification.

Table 4.13: Maximum stresses for each group in the FLS. Highlighted cells indicate highest stress of all groups.

AreaGroup	$\sigma_{x_{top}} (N/mm^2)$	$\sigma_{y_{top}} (N/mm^2)$	$\sigma_{x_{bot}} (N/mm^2)$	$\sigma_{y_{bot}} (N/mm^2)$
Group1	0.000270	0.000068	0.000211	0.000053
Group2	0.000864	0.000069	0.000754	0.000056
Group3	0.000834	0.000085	0.000768	0.000065
Group4	0.000747	0.000106	0.000712	0.000091
Group5	0.000701	0.000131	0.000671	0.000120
Group6	0.000656	0.000171	0.000624	0.000159
Group7	0.000621	0.000231	0.000603	0.000221
Group8	0.000594	0.000308	0.000571	0.000298
Group9	0.000580	0.000370	0.000567	0.000362
Group10	0.000563	0.000446	0.000544	0.000439
Group11	0.000566	0.000517	0.000555	0.000512
Group12	0.000555	0.000592	0.000538	0.000585
Group13	0.000548	0.000625	0.000534	0.000619
Group14	0.000546	0.000634	0.000535	0.000629
Group15	0.000533	0.000638	0.000524	0.000635
Group16	0.000559	0.000604	0.000549	0.000602
Group17	0.000624	0.000441	0.000629	0.000439
Group18	0.000683	0.000526	0.000669	0.000530
Group19	0.001607	0.001325	0.001001	0.000399

The rainflow count was attained from a wind turbine manufacturer according to Table 4.14.

Fatigue control was managed using the Palmgren-Miner's rule, with detail category 160 selected. The cumulative damage is indicated by the final value of table, 4.15 which is below 1. The values in the table have been rounded for clarity of presentation. With that said, cumulative damage may not necessarily equal the sum of the "Damage" column values for this table.

Table 4.14: Rainflow count by manufacturer.

(cont.)

Range [Nm]	Cycles
712,987	761,128,473.985	210,568,000	69.015
8,099,440	252,130,931.865	218,666,000	35.320
16,198,200	53,080,704.460	226,765,000	51.550
24,296,900	12,623,632.870	234,864,000	35.720
32,395,600	4,891,101.060	242,962,000	35.290
40,494,300	2,530,918.755	251,061,000	16.130
48,593,000	1,343,169.405	259,160,000	16.855
56,691,800	728,144.375	267,259,000	11.865
64,790,500	448,836.855	275,357,000	11.040
72,889,200	284,666.595	283,456,000	13.975
80,987,900	380,448.640	291,555,000	15.415
97,185,400	146,586.865	299,653,000	32.520
105,284,000	24,608.410	307,752,000	17.175
113,383,000	37,257.025	315,851,000	13.680
121,482,000	48,522.430	323,950,000	13.255
137,679,000	7,213.290	332,048,000	12.450
145,778,000	284.035	340,147,000	13.950
153,876,000	84.990	348,246,000	11.225
161,975,000	41.185	356,345,000	7.225
170,074,000	668.620	364,443,000	2.530
178,173,000	621.820	372,542,000	1.825
186,271,000	16.350	380,641,000	1.825
194,370,000	23.705	388,739,000	0.555
202,469,000	21.560	396,838,000	2.285
..	..	404,937,000	1.340

Table 4.15: Fatigue verification check with summarized cumulative damage. "inf" indicate infinite amount cycles to failure.

$\Delta\sigma_r$ (MPa)	Cycles to failure N_f (10^3)	Cycles measured n (10^3)	Damage (10^{-3})
0.001146	inf	761128.473	0.000000
13.015	inf	252130.932	0.000000
26.029	inf	53080.704	0.000000
39.043	inf	12623.633	0.000000
52.057	inf	4891.101	0.000000
65.070	97717.756	2530.919	0.025900
78.085	39271.221	134.3169	0.034202
91.099	18169.448	728.144	0.040075
104.113	9319.364	448.837	0.048162
117.127	5171.625	284.667	0.055044
130.141	3716.643	380.449	0.102364
156.169	2150.840	146.587	0.068153
169.182	1691.703	24.608	0.014547
182.197	1354.464	37.257	0.027507
195.211	1101.223	48.522	0.044062
221.238	756.498	7.213	0.009535
234.253	637.287	0.284	0.000446
247.266	541.874	0.085	0.000157
260.280	464.587	0.041	0.000089
273.294	401.326	0.668	0.001666
286.309	349.048	0.621	0.001781
299.322	305.474	0.016	0.000054
312.336	268.858	0.023	0.000088
325.350	237.867	0.021	0.000091
338.365	211.462	0.069	0.000326
351.378	188.828	0.035	0.000187
364.392	169.310	0.051	0.000304
377.406	152.391	0.035	0.000234
390.419	137.656	0.035	0.000256
403.434	124.759	0.016	0.000129
416.448	113.424	0.016	0.000149
429.462	103.422	0.011	0.000115
442.475	94.563	0.011	0.000117
455.489	86.687	0.013	0.000161
468.504	79.661	0.015	0.000194
481.517	73.376	0.032	0.000443
494.531	67.734	0.017	0.000254
507.546	62.656	0.013	0.000218
520.560	58.073	0.013	0.000228
533.573	53.927	0.012	0.000231
546.587	50.166	0.013	0.000278
559.602	46.746	0.011	0.000240
572.616	43.631	0.007	0.000166
585.629	40.787	0.003	0.000062
598.643	38.184	0.002	0.000048
611.658	35.798	0.002	0.000051
624.670	33.607	0.001	0.000017
637.685	31.591	0.002	0.000072
650.699	29.733	0.001	0.000045
Cumulative damage			0.48 < 1

5 Discussion

This chapter aims to critically examine key assumptions underlying the obtained results and clarify aspects of the thesis that might affect the result. Following the structure of the thesis, it will commence with a review of the background, proceed to discuss the methodology, and culminate in the presentation and analysis of the results.

5.1 Background

The wind turbine design involves numerous components, many of which are beyond the scope of this thesis and have been omitted. Only key aspects of the design are discussed here, due to the additional work of writing an automated script. Notably, while foundation design typically involves modeling both soil and the foundation itself, this project focuses solely on the automation of design processes of the foundation. It's important to clarify that this thesis does not address geotechnical analysis, although it acknowledges the potential significance of such considerations.

5.1.1 Bearing capacity and rotation

The external script responsible for assessing overturning and bearing capacity should not be conflated with the main script used for modeling and outputting reinforcement and section forces. The evaluation of bearing capacity and risk for overturning is conducted separately, adhering to the DNV RISØ guidelines for wind turbine design. While this method is simplified, it remains straightforward to follow and ensures stability. The script performs these calculations to verify the bearing capacity, sliding and overturning risks before proceeding with the modeling process. Revised version of the script will merge the external to the main one.

5.1.2 Convergence study

The convergence study was made to evaluate the accuracy to computational time. As depicted in the figures the Moments doesn't seem to converge as fast as the normal forces. With finer meshing of the *PedestalGroup* it is believed that better results will be obtained.

5.1.3 Modelling

The modelling approach adopted in this study utilized thick area elements, chosen for their efficiency in facilitating faster and approximate calculations. While this method

served the purpose adequately, it raises questions regarding the accuracy of the results when compared to modelling with solid elements. The reason for the uncertainty aligns with the assumption that the bending appears in the same plane as the area element. This justifies considerations due to the area element plane being positioned at the bottom of the model with an assigned offset thickness to replicate a solid element behaviour. Despite this, no investigations into the potential discrepancies between thick area and solid element models have been conducted. It is imperative to assess the magnitude of error associated with modeling with thick area elements instead of solid elements. This aspect calls for additional exploration in future research and holds the potential to be the subject of a standalone thesis, or complement for this thesis richness.

The *PedestalGroup*, identified as the innermost group in Fig.4.5, is modeled to inherit the same properties as the surrounding element groups, which poses a significant limitation. Ideally, the pedestal group should accurately represent the properties of the anchor cage. However, in this thesis, the anchor cage is simplified by applying only a rigid body constraint to the nearest nodes of the *PedestalGroup*. This results in compression in an area next to the *PedestalGroup* and tension in the opposite part, Fig. 4.6a. This constraint becomes particularly evident when observing Fig. E.2a, where the *PedestalGroup* exhibits a rotating behavior. Even though the anchor cage has been simplified in this manner it still yields a desired behaviour of the model.

Another important aspect of the modeling behavior is the tendency of the entire foundation to tip over. Figure 5.1 presents a scaled representation of the displacement in the Ultimate Limit State (ULS), showing an overturning moment to the right. While not immediately apparent, the *PedestalGroup* appears to tilt even more than the foundation itself. This observation justifies that the body constrained nodes are applied and the anchor cage is the cause of overturning. It can be concluded that additional investigation into the anchor cage and its interaction with the surrounding concrete is necessary for future endeavors.

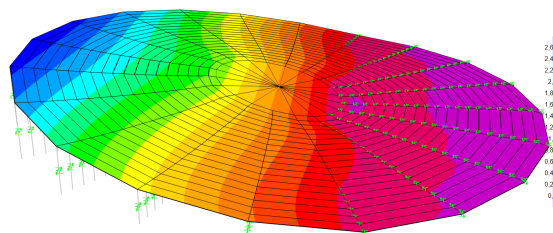


Figure 5.1: Scaled deformation of the displacement in the vertical direction.

Furthermore, it should be noted that a revised script will include meshing of the pedestal group, which will provide more detailed insight in its behaviour.

5.1.4 Loads

As mentioned in the limitations the dead load was not applied separately before gradually increasing the live load for the analysis. The rationale behind this approach lies in the importance of understanding the structure's response to the dead load, which

serves as a baseline. Additionally, incrementally increasing the load allows for observing the structure's behavior under varying levels of loading, particularly relevant for nonlinear loading scenarios. Despite the motivation to follow this procedure it was not performed. Acknowledging this limitation, future studies could explore this approach in providing a more comprehensive understanding of structural behavior under nonlinear loading conditions.

5.1.5 Springs

Another aspect in the modeling process that is in need of great detail is the determination of the spring stiffness in the vertical and horizontal directions. In a real-case it's possible to do soil investigations which will yield a more thorough result for that particular case. Such a survey is however, costly hence an approximate value for the spring stiffness according to the literature is to prefer. The DNV RISØ often referenced to, has a clear explanation on how the spring stiffness can be determined, hence it was the one used for this thesis. With that being said it would be great however to have a revised version considering it dating back to 2004.

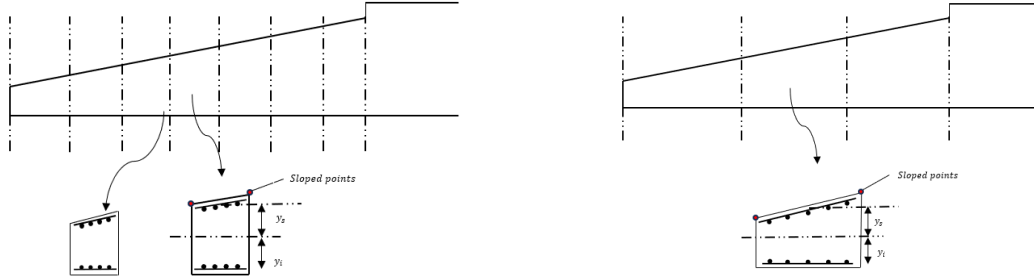
The DNV RISØ employs different scenarios depending on whether or not the foundation is embedded, and account for the characteristics of the soil layer beneath the excavated one. For a more conservative analysis, it's advisable to calculate the spring stiffness for the non-embedded case, Fig. 2.7. In this scenario, the restriction of horizontal movement by the soil is not considered, except for the friction between the foundation and the soil. As a result, this approach yields a lower spring stiffness value.

The results are dependent on the spring stiffness, a parameter easily changeable within the script. This can be accomplished by either creating a new function based on chosen literature or by directly assigning a value to the spring stiffness variable. This thesis does not explore the direct impact of the springs. Nevertheless, experiments with significantly higher spring stiffness demonstrated a decreased requirement for the reinforcement area in the radial and tangential direction. This observation aligns with the understanding that soil modeled with high spring stiffness provides enhanced support and stability, reducing the necessity for additional reinforcement due to the foundation encountering less displacements.

5.1.6 Reinforcement

The calculation of the reinforcement followed the sandwich model, section 2.5.2. This model simplifies the conversion of section moments into section normal forces by dividing them by a lever arm, z , which is the distance from the reinforcement steel at the top to bottom, Fig 2.10. Due to the incline of the foundation, the sandwich model was modified slightly. The inclination of the area elements gives rise to the fact that the superior distance, y_s , always yields an error. In the script, the superior height of the area element is set to the average height between the two inclined points relative to the center of the area element thickness. This will generate an error if one uses a coarse mesh, due to the *sloped points* being further apart. However, one could argue that with the use of a finer mesh, say an infinite one, the *sloped points* would become

practically indistinguishable from one another, and the mean height would correspond to the *sloped points*. This phenomenon is displayed in, Fig 5.2. The same reasoning applies for determining the center of the area element. One is therefore safe to say that the superior distance is not affected, thus won't yield any error if one uses a fine mesh.



(a) The effect of a finer mesh.

(b) The effect of a coarser mesh.

Figure 5.2: A schematic representation illustrating the assumption that utilizing the mean height for the sloped points for y_s has a negligible impact on the outcome when employing a finer mesh.

Two additional assumptions incorporated into the script for reinforcement design, which are believed to have minimal impact on the results, are as follows:

- The first assumption involves averaging the top and bottom reinforcement diameters when computing z , as illustrated in Fig 2.10. This effect is considered to have minimal impact on the results due to the small distance relative to the foundation.
- The second assumption assumes that the tangential and radial reinforcement work in the same plane, as depicted in Fig 5.3.



Figure 5.3: Schematic view of the assumption of having reinforcement in the same plane

The impact of these two assumptions is considered minor and thus not further investigated, but are mentioned for completeness.

The sandwich model is structured such that the outer layers bear the effects of bending and twisting moments, while the inner layer handles transverse shear forces. This assumes that the inner concrete layer can withstand the shear forces without cracking. While investigating this behavior could be necessary to verify the concrete's capacity in plane, incorporating such verification into the script could be a significant improvement. However, for the purposes of this thesis, the risk of shear cracking in the plane is deemed unlikely. This decision is motivated by considering the foundation in 2D, which behaves similarly to a concrete beam. In such cases, it's uncommon for a concrete beam to split in the lengthwise direction before the vertical.

5.2 Fatigue

The fatigue verification follows the Palmgren-Miner rule, which is a linear model. In addition, it was issued in the most simple manner where mean stress values for each stress range was neglected. In future work, exploring the impact of considering mean stresses within each stress range is of interest for a more comprehensive fatigue assessment. As it seems to be industry standard for civil structures it is not deemed relevant for this thesis.

The Palmgren-Miner rule was introduced 1926 which questions its relevance. It would hence be interesting to study other fatigue assessment methods which could be incorporated by the script. It must be mentioned, however, that more advanced models do not necessarily yield a better result. Not only because the risk of making an error increases, but also interpretation and communicating falls short with the increase of complexity.

The result, Table 4.15, indicates that the cumulative damage is less than 1, $0.48 < 1$. This verifies that no risk for fatigue is present. However, what is necessary to mention is that the fatigue verification neglects what combination of stress range contributes to the most damage. One only assumes that the highest stress range amplitudes are the one that generates the most damage.

The SN curve used for the fatigue verification follows the one from EN 1993-1-9, which doesn't comply with reinforcement fatigue that is being assessed. The detail category 160 that was assumed for this thesis is the highest, meaning that no detail can achieve better fatigue strength in any number of cycles. For a more conservative result one can choose a lower detail category such as, 80 in the script. This will generate a SN curve with lower value, hence increasing the cumulative damage.

For a better result one could argue to do specimen tests on reinforced concrete but the outcome of that is unclear. Given this, the fatigue assessment should be approached with caution. Moreover, the process of how it can be approached should motivate further automation of fatigue computation.

5.3 Final words

This thesis has focused on the development of an automated script intended to model and design a wind turbine foundation. How such a design can be approached has been discussed and will serve as a foundation for future advancements. The script has been created with the same structure as the method with added background features. Moving forward, the emphasis will be on refining the automated model while also endeavoring to create a merged script capable of generating a Parametric model in Tekla Structures. This work represents a step toward streamlining the design process, contributing to the ongoing digitalization of infrastructure.

Bibliography

- [1] Renewable energy. “Wind turbine orders rise to record 69.5 GW in H1, says WoodMac”. In: (2023).
- [2] Lucía Fernández. “Global investments in wind energy technologies reached roughly 175 billion U.S.” In: (2023).
- [3] IEA. *Analysis and forecast to 2028*. Tech. rep. IEA, 2023.
- [4] A.Scassola I.Buckland J. Lee F. Zhao A. Lathigara. *Global Wind Workforce Outlook*. Tech. rep. Global Wind Energy Council, 2023.
- [5] Erich Hau. *Wind Turbines*. Springer Berlin, Heidelberg, 2013.
- [6] <http://www.steelwindtower.com/onshore-wind-tower-foundation-types/>. Accessed: 2024-02-28.
- [7] Risø National Laboratory Wind Energy Department. *Guidelines for Design Of Windturbines*. Tech. rep. DNV-RISØ, 2002.
- [8] Bengt H. Fellenius. *Basics of Foundation Design*. Lulu.com, 2019.
- [9] Joachim Göhlmann Jürgen Grünberg. *Concrete Structures for Wind Turbines*. Erns Sohn, 2013.
- [10] B.S. Choo P.Bhat T.J MacGinley. *Reinforced concrete design to Eurocodes*. Taylor Francis, 2014.
- [11] Oldrich Sucharda Martina Smirakova Jana Vaskova Pavline Mateckova Jan Kubosek and Radim Cajka. “Punching Shear Failure of Concrete Ground Supported Slab”. In: (2018).
- [12] P.Lukás M.Klesnil. *Fatigue of metallic materials*.
- [13] J. J. Kauzlarich. *The Palmgren-Miner rule derived*. Tech. rep.
- [14] J.J. Barradas Berglind and Rafael Wisniewski. *FATIGUE ESTIMATION METHODS COMPARISON FOR WIND TURBINE CONTROL*. 3 March 2016.
- [15] Dowling NE. “Fatigue failure predicitions for complicated stress-strain histories”. In: *DTIC Document* (1971).
- [16] Sutherland H. *On the Fatigue Analysis of Wind Turbines*. Tech. rep. Sandia National Laboratories: Albuquerque, New Mexico, 1999.
- [17] Lee Y Pan J Hathaway R Barkey M. *Fatigue Testing and Analysis: Theory and Practice*. Butterworth-Heinemann: United States of America, 2005.
- [18] I. Rychlik. “Simulation of Load Sequences from Rainflow Matrices: Markov Method,” in: *International Journal of Fatigue*, vol. 18, no. 7, pp. 429–438 (1996).
- [19] ATM E1049-85. “Standard Practices for Cycle Counting in Fatigue Analysis”. In: *West Conshohocken, PA: ASTM International* (2017).

- [20] *About shell elements*. Tech. rep. Virginia Polytechnic Institute and State University, 2022. URL: <https://docs.software.vt.edu/abaqusv2022/English/SIMACAEELMRefMap/simaelm-c-shelloverview.htm>.

Appendix A

IEC Design load cases

Table A.1: Example of the IEC Load case Table.

Design situation	DLC	Wind condition	Other conditions	Type of analysis	Partial safety factors
1) Power Production	1.1	NTM	For extrapolation of extreme events	U	N
	1.2	NTM		F	
	1.3	ETM		U	N
	1.4	ECD		U	N
	1.5	EWS		U	N
2) Power Production plus occurrence of fault	2.1	NTM	Control system fault or loss of electrical network	U	N
	2.2	NTM	Protection system or preceding internal electrical fault	U	A
	2.3	EOG		U	A
	2.4	NTM	Control, protection, or electrical system faults	F	
3) Start up	3.1	NWP		F	
	3.2	EOG		U	N
	3.3	EDC		U	N
4) Normal shut down	4.1	NWP		F	
	4.2	EOG		U	N
5) Emergency shut down	5.1	NTM		U	N
6) Parked	6.1	EWM		U	N
	6.2	EWM		U	A
	6.3	EWM		U	N
	6.4	NTM		F	
7) Parked and fault conditions	7.1	EWM		U	A
8) Transport, assembly, maintenance and repair	8.1	NTM		U	T
	8.2	EWM		U	A

Appendix B

Bearing capacity

Drained conditions

Effective cohesion:

$$c' = \frac{c}{\gamma_{\gamma'_c}}$$

where

c cohesion

$\gamma_{\gamma'_c}$ Partial safety factor for effective cohesion EKS11

Design effective pressure at the level of foundation base:

$$p_0 = \frac{q}{\gamma_{\gamma}}$$

where

q surcharge pressure at the level of the foundation base.

γ_{γ} partial safety factor for weight density EKS11

Bearing capacity factors N :

$$N_q = e^{\pi \tan \phi_d} \cdot \frac{1 + \sin \phi_d}{1 - \sin \phi_d}$$

$$N_c = (N_q - 1) \cdot \cot(\phi_d)$$

$$N_{\gamma} = \frac{1}{4} \cdot ((N_q - 1) \cos(\phi_d))^{\frac{3}{2}}$$

According to Hansen (1970), N_{γ} may alternatively be calculated according to:

$$N_{\gamma} = \frac{3}{2} \cdot (N_q - 1) \cdot \tan^2(\phi_d)$$

Shape factors s :

$$s_{\gamma} = 1 - 0.4 \cdot \frac{b_{eff}}{l_{eff}}$$

$$s_q = s_c = 1 + 0.2 \cdot \frac{b_{eff}}{l_{eff}}$$

Inclination factors i :

$$i_q = i_c \left(1 - \frac{H_d}{V_d + A_{eff} \cdot c_d \cot \phi_d} \right)^m$$

$$i_q = i_c \left(1 - \frac{H_d}{V_d + A_{eff} \cdot c_d \cot \phi_d} \right)^m$$

$$i_\gamma = i_q^{m+1}$$

In the case of extreme eccentric loading, i.e., $e > 0.3b$, an additional bearing capacity calculation needs to be carried out. This failure mode refers to failures of the soil under the unloaded part of the foundation area. The following bearing capacity formula applies:

$$q_d = \gamma' b_{eff} N_\gamma s_\gamma i_\gamma + c_d N_c s_c i_c (1.05 + \tan^3 \phi)$$

where the corresponding inclination factors are:

$$i_q = i_c = 1 + \frac{H}{V + A_{eff} \cdot c \cdot \cot \phi}$$

$$i_\gamma = i_q^2$$

$$i_c^0 = \sqrt{0.5 + 0.5 \sqrt{1 + \frac{H}{A_{eff} \cdot c_{ud}}}}$$

Appendix C

Shear reinforcement

Shear Capacity without Shear Reinforcement

Parameters:

$C_{Rd,c}$ Reduction factor for concrete strength: $C_{Rd,c} = \frac{0.18}{(\gamma_c = 1.5)} = 0.12$

k Factor accounting for concrete crushing: $k = 1 + \sqrt{\frac{200}{d}} \leq 2.0$

ρ_1 Ratio of area of bending reinforcement in the tension zone to the product of width and effective depth: $\rho_1 = \frac{A_{sl}}{b_w d} \leq 0.02$

k_1 Constant factor: $k_1 = 0.15$

A_{sl} Area of tensile reinforcement extending beyond the shear section: (design anchorage length l_{bd} + effective depth)

v_{\min} Minimum shear reinforcement: $v_{\min} = 0.035k^{1.5}\sqrt{f_{ck}}$

σ_{cp} Axial compressive force: $\frac{P_s}{A_c} \leq 0.2f_{cd}$

Shear Capacity with Shear Reinforcement SS-EN 1992-1-1:2005 (E), section 6.2.3

Note 1: The recommended value of ν_1 is ν , see **Note 2**.

Note 2: If the design stress of the shear reinforcement is below 80% of the characteristic yield stress f_{yk} , ν_1 may be taken as:

$$\nu_1 = 0.6 \quad \text{for } f_{ck} \leq 60 \text{ MPa}$$

$$\nu_1 = 0.9 - \frac{f_{ck}}{200} > 0.5 \quad \text{for } f_{ck} > 60 \text{ MPa}$$

Note 3: The recommended value of α_{cw} is as follows:

$$1 \quad \text{for non-prestressed structures}$$

$$\left(1 + \frac{\sigma_{cp}}{f_{cd}}\right) \quad \text{for } 0 < \sigma_{cp} \leq 0.25f_{cd}$$

$$1.25 \quad \text{for } 0.25f_{cd} < \sigma_{cp} \leq 0.5f_{cd}$$

$$2.5\left(1 - \frac{\sigma_{cp}}{f_{cd}}\right) \quad \text{for } 0.5f_{cd} < \sigma_{cp} < f_{cd}$$

where: σ_{cp} is the mean compressive stress, measured positive, in the concrete due to the design axial force. This should be obtained by averaging it over the concrete section taking account of the reinforcement. The value of σ_{cp} need not be calculated at a distance less than $0.5d \cot T$ from the edge of the support.

Note 4: The maximum effective cross-sectional area of the shear reinforcement, $A_{sw,max}$, for $\cot \theta = 1$ is given by:

$$\frac{A_{sw,max} f_{ywd}}{b_w s} \leq \frac{1}{2} \alpha_{cw} \nu_1 f_{cd}$$

Parameters:

A_{sw}	Cross-sectional area of the shear reinforcement
θ	Inclination of the concrete strut to the beam axis ($1 \leq \cot \theta \leq 2.5$)
s	Spacing of links
f_{ywd}	Design yield strength of shear reinforcement
ν_1	Strength reduction factor for concrete cracked in shear ($0.6 \times (1 - \frac{f_{ck}}{250})$)
α_{cw}	Coefficient based on concrete compressive strength:
	For $0 < \frac{\sigma_{cp}}{f_{cd}} \leq 0.25$: $\alpha_{cw} = (1 + \frac{\sigma_{cp}}{f_{cd}})$
	For $0.25 < \frac{\sigma_{cp}}{f_{cd}} \leq 0.5$: $\alpha_{cw} = 1.25$
	For $0.5 < \frac{\sigma_{cp}}{f_{cd}} \leq 1.0$: $\alpha_{cw} = 0.25 \times (1 - \frac{\sigma_{cp}}{f_{cd}})$

Punching

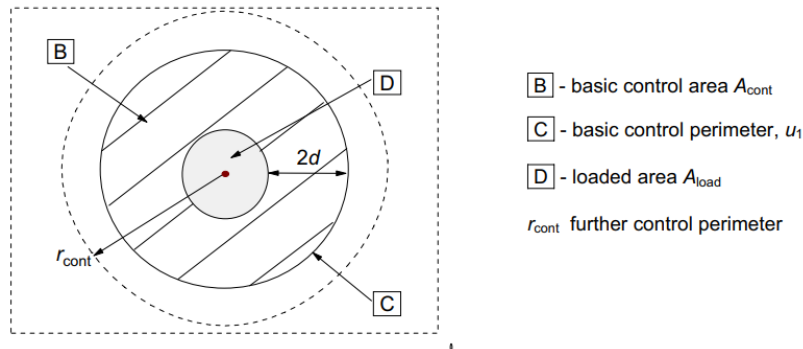


Figure C.1: Punching area, SS-EN-1992-1-1:2005

For internal circular column β

$$\beta = 1 + 0.6\pi \frac{e}{D+4d}$$

where

e is the distance of d from the axis about which the Moment, M_{Ed} acts
 D is the diameter of the of the pedestal

Appendix D

Reinforcement example for sandwich model

Example provided by Reinforced Concrete design to Eurocodes, fourth edition, by P.Bhatt, T.J. MacGinley, B.S.Choo.

Design the necessary reinforcement for a slab 500 mm thick subjected to the following combination of forces at the ultimate limit state. Assume $f_{yd} = 435$ MPa, $f_{cd} = 20$ MPa, and $\nu f_{cd} = 10.56$ MPa:

$$N_x = 1000 \text{ N/mm}, N_y = 1400 \text{ N/mm}, N_{xy} = 900 \text{ N/mm}$$

$$M_x = 60 \text{ kNm/m}, M_y = 100 \text{ kNm/m}, M_{xy} = 60 \text{ kNm/m}$$

Assume cover to steel = 30 mm, reinforcement H20.

Solution:

(i) Take average values only.

Thickness of top and bottom layers = $2 \times 30 + 20 = 80$ mm

$$z = 500 - 80 = 420 \text{ mm}$$

$$y_s = y_i = z/2 = 210 \text{ mm}$$

(ii) Determine the in-plane forces in the top and bottom layers due to applied force and moments.

$$M_x/z = \frac{60 \times 10^6}{10^3 \times z} = 143 \text{ N/mm},$$

$$M_y/z = \frac{100 \times 10^6}{10^3 \times z} = 238 \text{ N/mm},$$

$$M_{xy}/z = \frac{100 \times 10^6}{10^3 \times z} = 238 \text{ N/mm},$$

$$N_x(1 - y_s/z) = N_x(1 - y_i/z) = 500 \text{ N/mm},$$

$$N_y(1 - y_s/z) = N_y(1 - y_i/z) = 700 \text{ N/mm},$$

$$N_{xy}(1 - y_s/z) = N_{xy}(1 - y_i/z) = 450 \text{ N/mm}.$$

(iii) Design of reinforcement

Top layer:

$$\begin{aligned}
N_x &= 500 - 143 = 357 \text{ N/mm}, \\
N_y &= 700 - 238 = 462 \text{ N/mm}, \\
N_{xy} &= 450 - 238 = 212 \text{ N/mm},
\end{aligned}$$

$$\begin{aligned}
\frac{N_x}{|N_{xy}|} &= 1.68, & \frac{N_y}{|N_{xy}|} &= 2.18, & \frac{N_x N_y}{N_{xy}^2} &= 3.66, \\
\text{As } \frac{N_x}{|N_{xy}|} &> -1 \text{ and } \frac{N_y}{|N_{xy}|} &> -1, \text{ this falls into case 3.}
\end{aligned}$$

$$\begin{aligned}
A_x f_{yd} &= N_x + |N_{xy}| = 569, & A_x &= 1.31 \text{ mm}^2/\text{mm}, \\
\text{Provide H20 at 225 mm c/c giving} &= 1.40 \text{ mm}^2/\text{mm}.
\end{aligned}$$

$$\begin{aligned}
A_y f_{yd} &= N_y + |N_{xy}| = 674, & A_x &= 1.55 \text{ mm}^2/\text{mm}, \\
\text{Provide H20 at 200 mm c/c giving} &= 1.57 \text{ mm}^2/\text{mm}.
\end{aligned}$$

$$N_2 = -2|N_{xy}| = -424 \text{ N/mm}, \quad t = 80 \text{ mm}, \quad \sigma^2 = \frac{N^2}{t} = -5.3 \text{ MPa}.$$

Maximum compressive stress is less than νf_{cd} .

Bottom layer:

$$\begin{aligned}
N_x &= 500 + 143 = 643 \text{ N/mm}, \\
N_y &= 700 + 238 = 938 \text{ N/mm}, \\
N_{xy} &= 450 + 238 = 688 \text{ N/mm},
\end{aligned}$$

$$\begin{aligned}
\frac{N_x}{|N_{xy}|} &= 0.93, & \frac{N_y}{|N_{xy}|} &= 1.36, & \frac{N_x N_y}{N_{xy}^2} &= 1.27, \\
\text{As } \frac{N_x}{|N_{xy}|} &> -1 \text{ and } \frac{N_y}{|N_{xy}|} &> -1, \text{ this falls into case 3.}
\end{aligned}$$

$$\begin{aligned}
A_x f_{yd} &= N_x + |N_{xy}| = 1331, & A_x &= 3.06 \text{ mm}^2/\text{mm}, \\
\text{Provide H20 at 100 mm c/c giving} &= 3.14 \text{ mm}^2/\text{mm}.
\end{aligned}$$

$$\begin{aligned}
A_y f_{yd} &= N_y + |N_{xy}| = 1626, & A_x &= 3.74 \text{ mm}^2/\text{mm}, \\
\text{Provide H20 at 80 mm c/c giving} &= 3.93 \text{ mm}^2/\text{mm}.
\end{aligned}$$

$$N_2 = -2|N_{xy}| = -1376 \text{ N/mm}, \quad t = 80 \text{ mm}, \quad \sigma^2 = \frac{N^2}{t} = -17.2 \text{ MPa},$$

Maximum compressive stress is greater than νf_{cd} .

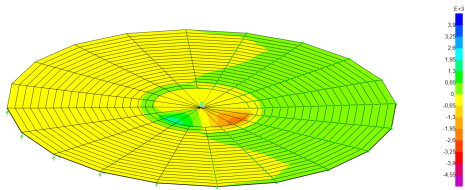
This stress is not a real stress. It is more a reflection of the modelling used.

Design is satisfactory.

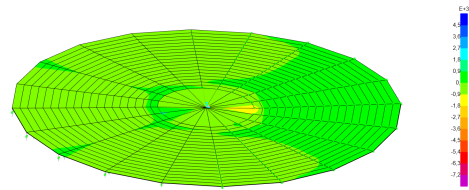
Appendix E

Load case results

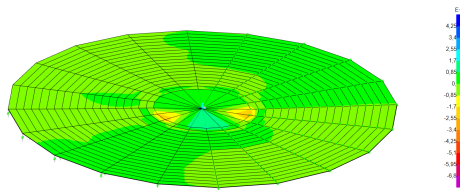
The first figures E.1 is the continued illustration of the Ultimate Limit State load case.



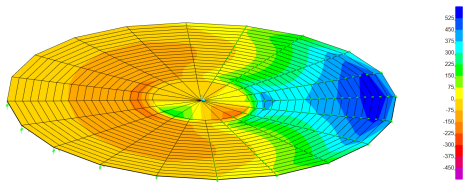
(a) M11 ULS



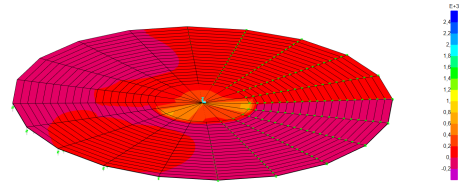
(b) M22 ULS



(c) M12 ULS



(d) V13 ULS



(e) V23 ULS

Figure E.1: Illustrative figures of the Ultimate Limit State load case.

Table E.1: Max value forces and corresponding forces for Fatigue load case, units of kN/m and kNm/m.

AreaLabel	OutputCase	F11	F22	F12	M11	M22	M12	V13	V23
378	FLS	0.6871	0.1413	0.2688	0.0029	0.0006	0.0006	0.0104	0.0006
360	FLS	-34.094	30.5023	12.1438	1.3890	0.3137	0.2396	4.9024	1.5612
344	FLS	-77.1965	-6.362	27.5195	-1.3110	-0.3207	-0.2888	5.9086	-1.4618
397	FLS	-35.1313	-25.0581	-18.294	59.9082	5.4694	4.5480	-13.1472	11.1035
392	FLS	-7.7149	-23.2323	9.5037	8.610	68.8454	-8.6068	-4.0294	35.9978
399	FLS	-20.6206	-25.0696	-3.1796	38.1418	18.632	12.1736	-8.6688	-28.3407
343	FLS	-68.8070	24.3251	14.1314	1.7616	0.3917	0.347	6.5985	0.0141
392	FLS	-7.7149	-23.2323	9.5037	8.6100	68.8454	-8.6068	-4.029	35.9978

Table E.2: Min value forces and corresponding forces for Fatigue load case, units of kN/m and kNm/m.

AreaLabel	OutputCase	F11	F22	F12(kN/m)	M11	M22	M12	V13	V23
342	FLS	-77.2251	-6.2244	-27.3758	-1.3116	-0.3208	0.2889	5.9127	1.4804
392	FLS	-9.7977	-32.5318	10.6762	20.7664	36.1885	-3.0910	-4.0294	35.9978
357	FLS	-76.9213	-6.3736	-27.4528	-1.3057	-0.3192	0.2874	5.8825	1.4590
393	FLS	-18.7661	-27.9475	14.1266	-6.4395	-2.2305	-9.3269	-9.7975	14.5157
399	FLS	-21.3174	-26.7446	-2.1264	-5.8729	-11.1449	11.5954	-8.6688	-28.3407
394	FLS	-31.0750	-23.9425	22.2752	48.6135	10.8066	-9.8675	-11.0487	-5.8558
398	FLS	-26.0170	-28.3657	-8.8619	-4.6858	-7.8114	7.1829	-13.1709	-8.2451
399	FLS	-21.3174	-26.7446	-2.1264	-5.8729	-11.1449	11.5954	-8.6688	-28.3407

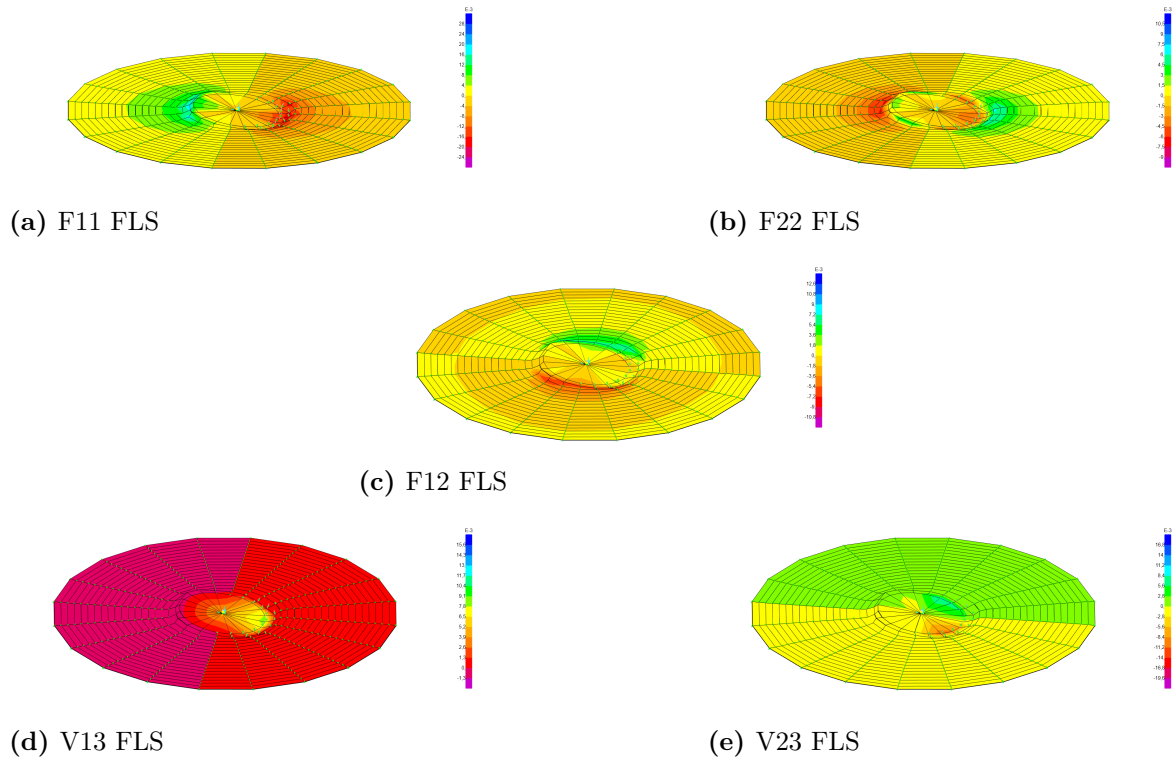


Figure E.2: FLS Variants.

Table E.3: Max value forces and corresponding forces for Serviceability load case, units of kN/m and kNm/m.

AreaLabel	OutputCase	F11	F22	F12	M11	M22	M12	V13	V23
378	SLS	0.69	0.14	0.27	0.00	0.00	0.00	0.01	0.00
360	SLS	-34.05	30.50	12.13	1.39	0.31	0.24	4.90	1.56
359	SLS	-76.96	-6.20	27.47	-1.31	-0.32	-0.29	5.90	-1.48
397	SLS	-35.17	-25.09	-18.34	59.78	5.47	4.50	-13.11	11.15
392	SLS	-7.73	-23.24	9.54	8.59	68.67	-8.63	-4.02	35.90
399	SLS	-20.62	-25.12	-3.20	38.10	18.59	12.13	-8.66	-28.30
343	SLS	-68.67	24.33	14.09	1.76	0.39	0.35	6.59	0.01
392	SLS	-7.73	-23.24	9.54	8.59	68.67	-8.63	-4.02	35.90

Table E.4: Min value forces and corresponding forces for Serviceability load case, units of kN/m and kNm/m.

AreaLabel	OutputCase	F11	F22	F12	M11	M22	M12	V13	V23
342	SLS	-77.11	-6.23	-27.37	-1.31	-0.32	0.29	5.91	1.48
392	SLS	-9.82	-32.59	10.71	20.71	36.09	-3.05	-4.02	35.90
357	SLS	-76.95	-6.38	-27.48	-1.31	-0.32	0.29	5.88	1.46
393	SLS	-18.81	-27.98	14.16	-6.37	-2.18	-9.32	-9.76	14.45
399	SLS	-21.31	-26.79	-2.14	-5.84	-11.16	11.61	-8.66	-28.30
394	SLS	-31.14	-23.97	22.31	48.44	10.82	-9.83	-11.00	-5.90
398	SLS	-26.03	-28.41	-8.90	-4.63	-7.80	7.19	-13.14	-8.21
399	SLS	-21.31	-26.79	-2.14	-5.84	-11.16	11.61	-8.66	-28.30

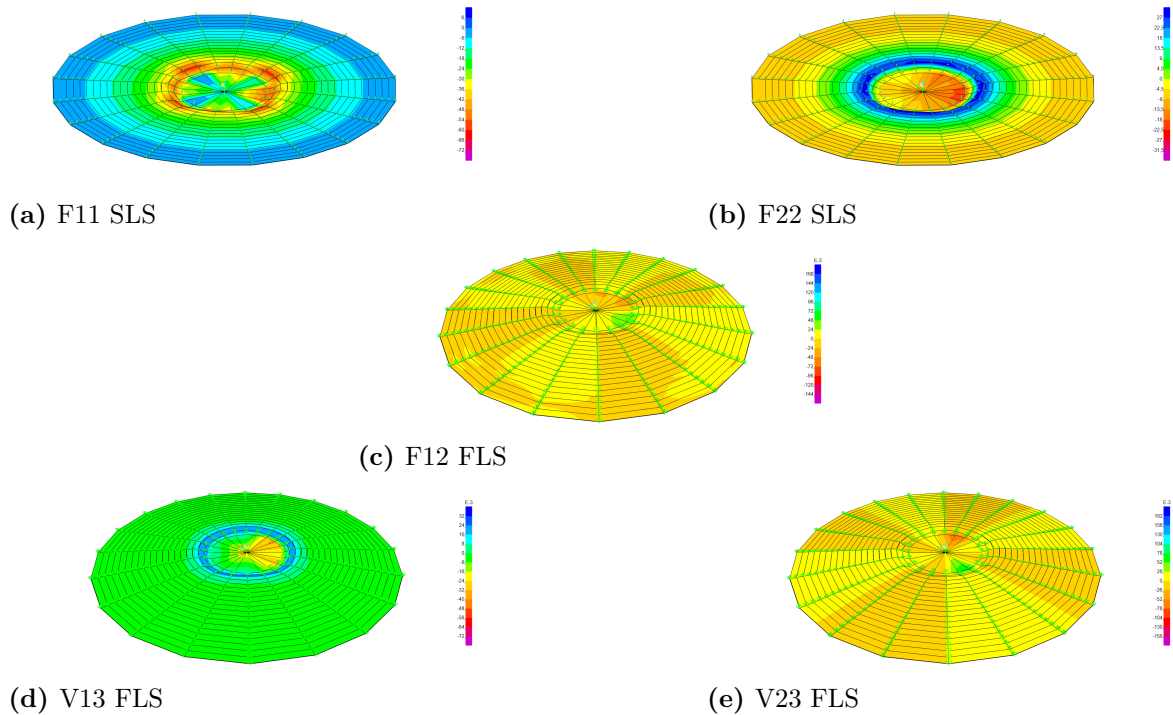


Figure E.3: FLS Variants.

Table E.5: Max value forces and corresponding forces for favourable load case, units of kN/m and kNm/m.

AreaLabel	OutputCase	F11	F22	F12	M11	M22	M12	V13	V23
348	EQU_Dead_favour	8335.04	2396.45	5632.73	-28.57	-2.22	3.18	-126.72	191.63
19	EQU_Dead_favour	837.68	11 414.58	-1819.29	174.43	48.91	1.90	382.60	-143.97
100	EQU_Dead_favour	-2931.94	892.28	10 351.66	110.40	-20.82	11.74	833.58	-284.80
392	EQU_Dead_favour	-906.10	1387.57	3010.12	21 587.02	3993.36	4546.82	2724.10	1756.83
392	EQU_Dead_favour	-215.11	4472.82	2621.14	-9985.22	4185.52	-6781.52	2724.10	1756.83
392	EQU_Dead_favour	-906.10	1387.57	3010.12	21 587.02	3993.36	4546.82	2724.10	1756.83
392	EQU_Dead_favour	-215.11	4472.82	2621.14	-9985.22	4185.52	-6781.52	2724.10	1756.83
400	EQU_Dead_favour	-1200.71	269.71	-3267.50	-4518.14	-961.41	-7844.62	-42.06	2491.14

Table E.6: Min value forces and corresponding forces for favourable load case, units of kN/m and kNm/m.

AreaLabel	OutputCase	F11	F22	F12	M11	M22	M12	V13	V23
361	EQU_Dead_favour	-26 961.67	-5366.52	-479.41	-75.41	-11.29	-13.31	238.30	212.54
379	EQU_Dead_favour	-20 006.00	-6948.89	6270.74	18.78	4.39	1.22	65.61	-56.52
81	EQU_Dead_favour	-3199.50	863.36	-10 270.78	115.32	-15.89	-11.97	842.05	278.22
383	EQU_Dead_favour	-0.32	-0.52	-0.13	-16 367.85	-762.53	-15.71	-2020.74	-3.81
400	EQU_Dead_favour	-1278.66	254.12	-3464.35	-1259.43	-8306.68	-8079.41	-42.06	2491.14
400	EQU_Dead_favour	-1278.66	254.12	-3464.35	-1259.43	-8306.68	-8079.41	-42.06	2491.14
398	EQU_Dead_favour	1079.57	-3797.33	2558.99	508.38	652.72	-917.76	-2127.60	591.67
20	EQU_Dead_favour	1826.26	-3431.73	6921.82	202.98	-10.15	25.75	1561.63	-404.17

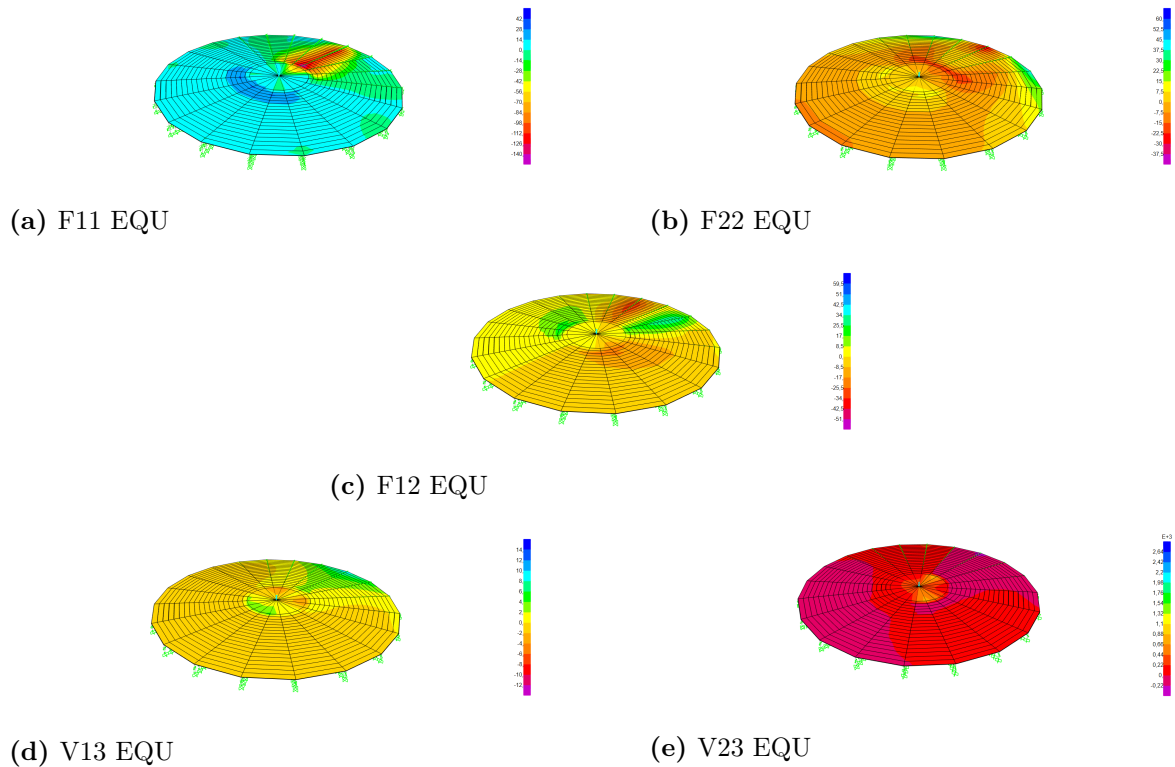


Figure E.4: EQU Variants.